DOE/ET/37240--T2

COO-2245-177R

Revision II

DOE/ET/37240--T2

DE82 007718

INPUT PARAMETERS TO CODES WHICH ANALYZE LMFBR WIRE-WRAPPED BUNDLES

(To be used with the ENERGY Code Manual)

By

E. U. Khan, W. M. Rohsenow, A. A. Sonin and
N. E. Todreas (May 1975)

Revision I: S. F. Wang and N. E. Todreas (May 1979)

Revision II: J. T. Hawley, Y. N. Chan and N. E. Todreas
(December 1980)

COO-2245-177R, Rev II

DISCLAIMER

N O T I C E

This report was prepared as an account of work sponsored by the United States Government. Neither the United States nor the Department of Energy, nor any of their employees, nor any of their contractors, subcontractors, or their employees, makes any warranty, express or implied, or assumes any legal liability or responsibility for the accuracy, completeness, or usefulness of any information, apparatus, product or process disclosed or represents that its use would not infringe privately-owned rights.

REPORTS AND PAPERS PUBLISHED UNDER MIT COOLANT MIXING IN LMFBR ROD BUNDLES PROJECT

A. Quarterly Progress Reports (Available from:
National Technical Information Service
U. S. Department of Commerce
Springfield, Virginia 22151)

COO-2245-1	Period June 1, 1972 - November 30, 1972
COO-2245-2	Period December 1, 1972 - February 28, 1973
COO-2245-3	Period March 1, 1973 - May 31, 1973
COO-2245-6	Period June 1, 1973 - August 31, 1973
COO-2245-7	Period September 1, 1973 - November 30, 1973
COO-2245-8	Period December 1, 1973 - February 28, 1974
COO-2245-10	Period March 1, 1974 - May 31, 1974
COO-2245-13	Period June 1, 1974 - August 31, 1974
COO-2245-14	Period September 1, 1974 - November 30, 1974
COO-2245-15	Period December 1, 1974 - February 28, 1975
COO-2245-23	Period March 1, 1975 - May 31, 1975
COO-2245-25	Period June 1, 1975 - August 31, 1975
COO-2245-26	Period September 1, 1975 - November 30, 1975
COO-2245-28	Period December 1, 1975 - February 29, 1976
COO-2245-30	Period March 1, 1976 - May 31, 1976
COO-2245-31	Period June 1, 1976 - August 31, 1976
COO-2245-34	Period September 1, 1976 - November 30, 1976
COO-2245-38	Period December 1, 1976 - February 28, 1977
COO-2245-50	Period March 1, 1977 - May 31, 1977
COO-2245-53	Period June 1, 1977 - August 31, 1977
COO-2245-60	Period September 1, 1977 - November 30, 1977
COO-2245-63	Period December 1, 1977 - February 28, 1978
COO-2245-64	Period March 1, 1978 - May 31, 1978
COO-2245-65	Period June 1, 1978 - August 31, 1978
COO-2245-66	Period September 1, 1978 - November 30, 1978

COO-2245-69 Period December 1, 1978-February 28, 1979

COO-2245-70 Period March 1, 1979-May 31, 1979

COO-2245-71 Period June 1, 1979-August 31, 1979

COO-2245-72 Period September 1, 1979-November 30, 1979

DOE/ET/37240-75 Period December 1, 1979-February 29, 1980

DOE/ET/37240-76 Period March 1, 1980-May 31, 1980

DOE/ET/37240-85 Period June 1, 1980-August 31, 1980

DOE/ET/37240-89 Period September 1, 1980-November 30, 1980

DOE/ET/37240-90 Period December 1, 1980-February 28, 1981

Reports Issued Under This Contract

B.1 Original Topical Reports (Available from National Technical Information Service, U.S. Department of Commerce, Springfield, VA 22151)

E. Khan and N. Todreas, "A Review of Recent Analytical and Experimental Studies Applicable to LMFBR Fuel and Blanket Assembly Design", COO-2245-4TR, MIT, September 1973.

E. Khan, W. Rohsenow, A. Sonin and N. Todreas, "A Simplified Approach for Predicting Temperature Distribution in Wire Wrapped Assemblies", COO-2245-5TR, MIT, September 1973.

T. Eaton and N. Todreas, "Instrumentation Methods for Interchannel Coolant Mixing Studies in Wire-Wrap Spaced Nuclear Fuel Assemblies", COO-2245-9TR, MIT, June 1974.

Y. B. Chen, K. Ip, N. E. Todreas, "Velocity Measurements in Edge Subchannels of Wire Wrapped LMFBR Fuel Assemblies", COO-2245-11TR, MIT, September 1974.

E. Khan, N. Todreas, W. Rohsenow, A. A. Sonin, "Analysis of Mixing Data Relevant to Wire-Wrapped Fuel Assembly Thermal-Hydraulic Design", COO-2245-12TR, MIT, September 1974.

E. Khan, W. Rohsenow, A. Sonin, N. Todreas, "A Porous Body Model for Predicting Temperature Distributions in Wire Wrapped Fuel and Blanket Assemblies of an LMFBR", COO-2245-16TR, MIT, June 1975.

* E. Khan, W. M. Rohsenow, A. Sonin, N. Todreas, "Input Parameters to the ENERGY Code (To be used with the ENERGY Codes Manual), COO-2245-17TR, MIT, May 1975.

* E. Khan, W. Rohsenow, A. Sonin, N. Todreas, "Manual for ENERGY Codes I, II, III", COO-2245-18TR, MIT, May 1975.

P. Carajilescov and N. Todreas, "Experimental and Analytical Study of Axial Turbulent Flows in an Interion Subchannel of a Bare Rod Bundle", COO-2245-19TR, MIT.

* B. Chen and N. Todreas, "Prediction of Coolant Temperature Field in a Breeder Reactor Including Interassembly Heat Transfer", COO-2245-20TR, MIT, May 1975.

* Revised - See Section B.2

B.1 Original Topical Reports (Continued)

F. Carre and N. Todreas, "Development of Input Data to ENERGY Code for Analysis of Reactor Fuel Bundles", COO-2245-21TR, MIT, May 1975.

H. Ninokata and N. E. Todreas, "Turbulent Momentum Exchange Coefficients for Reactor Fuel Bundle Analysis", COO-2245-22TR, MIT, June 1975.

R. Anoba and N. Todreas, "Coolant Mixing in LMFBR Rod Buncles and Outlet Plenum Mixing Transients, COO-2245-24TR, MIT, August 1975.

* B. Bosy, "Fabrication Details for Wire Wrapped Fuel Assembly Components", COO-2245-27TR, MIT, November 1975.

Ralph G. Bennett and Michael W. Golay, "Interferometric Investigation of Turbulently Fluctuating Temperature in an LMFBR Outlet Plenum Geometry", COO-2245-29TR, MIT, June 1976.

N. E. Todreas, "Thermal Analysis Methods for LMFBR Wire Wrapped Bundles", COO-2245-32TR, MIT, November 1976.

K. L. Basehore and N. E. Todreas, "Development of Stability Criteria and an Interassembly Conduction Model for the Thermal-Hydraulics Code SUPERENERGY", COO-2245-33TR, MIT, December 1976.

Robert Masterson and Neil E. Todreas, "Analysis of the Feasibility of Implementing an Implicit Temporal Differencing Scheme in the SUPERENERGY Code", COO-2245-35TR, MIT, February 1977.

S. Glazer, C. Chiu and N. Todreas, "Collection and Evaluation of Salt Mixing Data with the Real Time Data Acquisition System", COO-2245-36TR, MIT, April 1977.

B. Mikic, E. U. Khan and N. E. Todreas, "An Approximate Method for Predicting Temperature Distribution in Wire Wrapped Fuel Assemblies of an LMFBR", COO-2245-37TR, MIT, April 1977.

J. T. Hawley, C. Chiu and N. Todreas, "Development of a Technique for Subchannel Flow Rate Measurements in LMFBR Wire Wrapped Assemblies", to be issued as COO-2245-39TR 6/80. Never issued. Replaced by DOE/ET/37240-80TR.

* Revised - See Section B.2

B.1 Original Topical Reports (Continued)

* C. Chiu and N. Todreas, "WARD Blanket Assembly Pre-Test Predictions by SUPERENERGY", COO-2245-40TR, MIT, May 1977.

C. Chiu, N. Todreas, W. M. Rohsenow, "Flow Split Measurements in LMFBR Blanket Assemblies", COO-2245-41TR, MIT, April 1978.

C. Chiu, J. Hawley, W. M. Rohsenow and N. Todreas, "Pressure Drop Measurements in Wire Wrapped Blanket Assemblies", COO-2245-42TR, July 1977.

C. Chiu, W. M. Rohsenow and N. Todreas, "Mixing Experiments in LMFBR Wire Wrapped Blanket Assemblies", COO-2245-43TR, April 1978.

Yi Ben Chen and Michael W. Golay, "Coolant Mixing in the LMFBR Outlet Plenum", COO-2245-44TR, June 1977.

J. Kelly and N. Todreas, "Turbulent Interchange in Triangular Array Bare Rod Bundles", COO-2245-45TR, July 1977.

K. L. Basehore and N. E. Todreas, "Assessment of the Need to Incorporate a Variable Swirl Flow Model into the ENERGY Code", COO-2245-46TR, July 1977.

K. L. Basehore and N. Todreas, "Analysis of the Thermal-Hydraulic Behavior in the CRBR Secondary Control Assembly, Including Interassembly Heat Transfer Effects", COO-2245-47TR, July 1977.

J. G. Bartzis and N. E. Todreas, "Hydrodynamic Behavior of a Bare Rod Bundle", COO-2245-48TR, MIT, June 1977.

M. R. Fakori-Monazah and N. E. Todreas, "Measurement and Analysis of Flow Wall Shear Stress in an Interior Subchannel of Triangular Array Rods", COO-2245-49TR, MIT, August 1977.

* A. S. Hanson and N. E. Todreas, "Fluid Mixing Studies in an Hexagonal 61-Pin, Wire-Wrapped Rod Bundle", COO-2245-51TR, MIT, August 1977.

S. Glaser, N. Todreas, W. Rohsenow, and A. Sonin, "TRANSENERGY S - Computer Codes for Coolant Temperature Prediction in LMFBR Cores During Transient Events", COO-2245-52TR, MIT, February 1981.

C. Chiu, W. M. Rohsenow, and N. E. Todreas, "Mixing Experiments in an Alternating Wire Wrapped Assembly", COO-2245-54TR, MIT, December 1977.

* Revised - See Section B.2

B.1 Original Topical Reports (Continued)

* C. Chiu, W. M. Rohsenow and N. E. Todreas, "Turbulent Sweeping Flow Mixing Model for Wire Wrapped LMFBR Assemblies", COO-2245-55TR, MIT, April 1978.

* C. Chiu, W. M. Rohsenow and N. E. Todreas, "Flow Split Model for LMFBR Wire Wrapped Assemblies", COO-2245-56TR, MIT, April 1978.

K. Basehore and N. E. Todreas, "SUPERENERGY: Multiassembly Thermal-Hydraulic LMFBR Code", to be issued as Topical Report COO-2245-57TR, MIT, NED

C-N. Wong and L. Wolf, "A 3-D Slug Flow Heat Transfer Analysis of Coupled Coolant Cells in Finite LMFBR Bundles", COO-2245-58TR, MIT, February 1978.

Roohollah Karimi and L. Wolf, "Two Dimensional Structural Analysis of Reactor Fuel Element Claddings Due to Local Effects", COO-2245-59TR, MIT, April 1978.

Vincent Manno and Michael Golay, "Measurement of Heat and Momentum Eddy Diffusivities in Recirculating LMFBR Outlet Plenum Flows", COO-2245-61TR, MIT, June 1978.

* Hafeez Khan, Chong Chiu and Neil Todreas, "Laboratory Manual for Salt Mixing Test in Rod Bundles", COO-2245-62TR, MIT, October 1978.

J. Y. Kim and L. Wolf, "Fully-Developed Mixed Convection Heat Transfer and Pressure Drop in Characteristic Coolant Cells of Finite Hexagonal Bare Bundles", COO-2245-67TR, MIT, Dec. 1978.

M. K. Yeung and L. Wolf, "A Multicell Slug Flow Heat Transfer Analysis of Finite LMFBR Bundles", COO-2245-68TR, MIT, December 1978.

S. F. Wang, W. M. Rohsenow, N. E. Todreas, "Steady, Laminar, Fully-Developed Mixed Convection in Finite Rod Arrays", COO-2245-73TR, MIT, Feb. 1981.

P. D. Symolon, N. E. Todreas, "A Manual for Use with the Computer Code Superenergy-Data Reduction Version", COO-2245-74TR, MIT, February 1980.

K. J. Burns, N. E. Todreas, "Laboratory Manual for Static Pressure Drop Experiments in LMFBR Wire Wrapped Rod Bundles," DOE/ET/37240-77TR, July 1980.

K. J. Burns, N. E. Todreas, "A Comparison Between the SIMPLE and ENERGY Code Mixing Models," DOE/ET/37240-78TR, July 1980.

* Revised - See Section B.2

B.1 Original Topical Reports (Continued)

J. T. Hawley, C. Chiu, W. M. Rohsenow, N. E. Todreas, "Correlations for Subchannel and Bundle Friction Factors and Flowsplit Parameters for Laminar, Transition, and Turbulent Longitudinal Flows in Wire Wrap Spaced Hexagonal Arrays", DOE/ET/37240-79TR, Dec. 1980.

J. T. Hawley, C. Chiu, N. E. Todreas, "M.I.T. Extraction Method for Measuring Average Subchannel Axial Velocities in Reactor Assemblies", DOE/ET/37240-80TR, July 1980.

K. J. Burns, W. M. Rohsenow, N. E. Todreas, "Laminar/ Transition Sweeping Flow Mixing Model for Wire Wrapped LMFBR Assemblies", DOE/ET/37240-81TR, July 1980.

T.E. Greene, N. E. Todreas, "Criteria for Onset of Mixed Convection in Wire Wrap Spaced Hexagonal Arrays", Report DOE/ET/37240-82TR, to be issued.

D. R. Boyle and M. W. Golay, "Transient Effects in Turbulence Modelling", DOE/ET/37240-83TR , Feb. 1980.

P. D. Symolon and N. E. Todreas, "Fluid Mixing Studies in a Hexagonal 217 Pin Wire Wrapped Rod Bundle," DOE/ET/ 37240-84TR, Feb. 1981.

S. F. Wang, W. M. Rohsenow, and N. E. Todreas, "Flow Split, Pressure Drop, and Mixing Experiments in a 61 Pin Shaved-Wire Blanket Assembly, DOE/ET/37240-86TR, Feb. 1981.

S. F. Wang, N. E. Todreas, "Computer Model for M.I.T. Correlations for Friction Factors, Flow Split, and Mixing Parameters in LMFBR Wire-Wrapped Rod Assemblies, DOE/ET/ 37240-87TR, Feb. 1981.

S. F. Wang and N. E. Todreas, "Experimental Investigations of Laminar Mixed Convection in a Square Array of Bare Rods," Report No. DOE/ET/37240-88TR, Feb. 1981.

Reports Issued Under This Contract

B.2 Revised Topical Reports (Available from National Technical Information Service, U.S. Department of Commerce, Springfield, VA 22151)

S. F. Wang and N. E. Todreas, "Input Parameters to Codes Which Analyze LMFBR Wire-Wrapped Bundles," COO-2245-17TR, (Revision I), MIT, May, 1979.

** E. Khan, W. Rohsenow, A. Sonin, N. Todreas, "Manual for ENERGY Codes I, II, III Computer Programs", COO-2245-18TR, Revision I, MIT, July 1976.

** B. C. Chen and N. E. Todreas, "Prediction of Coolant Temperature Field in a Breeder Reactor Including Inter-assembly Heat Transfer," COO-2245-20TR, (Revision I), MIT, December, 1976.

H. Khan, "Fabrication Details for Wire-Wrapped Fuel Assembly Components," COO-2245-27TR, (Revision I), MIT, September, 1978.

** K. W. Chiu, "Fabrication Details for Wire-Wrapped Fuel Assembly Components," COO-2245-27TR, (Revision II), MIT, September, 1979.

C. Chiu, W. M. Rohsenow and N. E. Todreas, "Turbulent Sweeping Flow Mixing Model for Wire Wrapped LMFBR Assemblies", COO-2245-55TR, Rev. 1, MIT 1978.

** J. T. Hawley, Y. N. Chan and N. E. Todreas,"Input Parameters to Codes which Analyze LMFBR Wire Wrapped Bundles," COO-2245-17TR, (Revision II), December 1980.

** P. D. Symolon and N. E. Todreas, "Fluid Mixing Studies in a Hexagonal 61 Pin Wire Wrapped Rod Bundle," COO-2245-51TR, (Revision I), February 1981.

** Y. N. Chan and N. E. Todreas, "Turbulent Sweeping Flow Mixing Model for Wire Wrapped LMFBR Assemblies," COO-2245-55TR, (Revision II), December 1980.

** Y. N. Chan and N. E. Todreas, "Turbulent Flow Split Model and Supporting Experiments for Wire Wrapped Core Assemblies," COO-2245-56TR, (Revision I), December 1980.

** Y. N. Chan and N. E. Todreas, "Laboratory Manual for Salt Mixing Test in 37- and 217-Pin Bundles," COO-2245-62TR, (Revision I), August 1980.

** Latest Revision

B.2 Revised Topical Reports (Continued)

(Available from National Technical Information Service, U. S. Department of Commerce, Springfield, VA 22151)

** T. E. Greene and N. E. Todreas, "WARD Blanket Assembly Pre-Test Predictions by SUPERENERGY," COO-2245-40TR, Revision I, April 1981.

** Latest Revision

Reports Issued Under This Contract

C. Papers and Summaries

Y. B. Chen, K. L. Ip, and N. E. Todreas, "Velocity Measurements in Edge Channels of Wire-Wrapped LMFBR Fuel Assemblies," American Nuclear Society Transactions, Vol. 19, 1974, pp. 323-324.

P. Carajilescov and N. Todreas, "Experimental and Analytical Study of Axial Turbulent Flows in an Interior Subchannel of a Bare Rod Bundle," J. of Heat Transfer, Vol. 98, No. 2, May 1976, pp. 262-268, (Included as Appendix to Quarterly Progress Report, COO-2245-15).

E. Khan, W. Rohsenow, A. Sonin, and N. Todreas, "A Porous Body Model for Predicting Temperature Distribution in Wire-Wrapped Fuel Rod Assemblies," Nuclear Engineering and Design, 35 (1975), pp. 1-12.

E. Khan, W. Rohsenow, A. Sonin, and N. Todreas, "A Porous Body Model for Predicting Temperature Distribution in Wire-Wrapped Rod Assemblies Operating in Combined Forced and Free Convection," Nuclear Engineering and Design, 35 (1975), pp. 199-211.

R. G. Bennett and M. W. Golay, "Development of An Optical Method for Measurement of Temperature Fluctuation in Turbulent Flows," American Nuclear Society Transactions, Vol. 22, 1975, p. 581.

B. Chen and N. Todreas, "Prediction of the Coolant Temperature Field in a Breeder Reactor Including Interassembly Heat Transfer," Nuclear Engineering and Design, 35, (1975), pp. 423-440, (Included as Appendix to Quarterly Progress Report, COO-2245-23).

R. Bennett and M. W. Golay, "Interferometric Investigation of Turbulently Fluctuating Temperature in an LMFBR Outlet Plenum Geometry," Presented at the ASME Annual Winter Meeting, December, 1976, (Included as Appendix in Quarterly Progress Report, COO-2245-30).

B. B. Mikic, E. U. Khan, and N. E. Todreas, "An Approximate Method for Predicting Temperature Distribution in Wire-Wrapped Fuel Assemblies of a Liquid Metal Fast Breeder Reactor," Mech. Res. Comm., Vol. 3, (1976), pp. 353-360.

L. Wolf, R. Karimi, J. Y. Kim, C. N. Wong, and M. K. Yeung, "2-D Thermoelastic Analysis of LMFBR Fuel Rod Claddings," Paper C4/d, 4th International Conf. Structural Mechanics in Reactor Technology, San Francisco, August 1977.

Reports Issued Under This Contract

C. Papers and Summaries (Continued)

M. Yeung, and L. Wolf, "Effective Conduction Mixing Lengths for Subchannel Analysis of Finite Hexagonal LMFBR Bundles," Transactions of the American Nuclear Society, June 1977, Vol. 26, pp 463-464.

C. Chiu and N. Todreas, "Flow Split Measurements in an LMFBR Radial Blanket Assembly," Transactions of the American Nuclear Society, June 1977, Vol. 26, pp 455-456.

J. Y. Kim and L. Wolf, "Laminar Mixed Convection Heat Transfer in Finite Hexagonal Bundles," Transactions of the American Nuclear Society, (1977), Vol. 27, pp 384-385.

J. Kelly and N. Todreas, "Turbulent Interchange in Triangular Array Bare Rod Bundles," Paper NR-3, Presented at Sixth International Heat Transfer Conference, Toronto, August 1978.

C. Chiu, N. E. Todreas, and W. M. Rohsenow, "Turbulent Flow Split Experiment and Model for Wire-Wrapped Assemblies," Transactions of the American Nuclear Society, June, 1978, Vol. 28, TANSAO 28, (1978), pp 536-537, ISSN: 0003-018X.

C. Chiu, N. E. Todreas, and W. M. Rohsenow, "Pressure Drop Measurements in LMFBR Wire-Wrapped Blanket Bundles," Transactions of the American Nuclear Society, Vol. 30, pp 541-543, (1978).

C. Chiu, N. E. Todreas, and W. M. Rohsenow, "Turbulent Mixing Experiment and Model for Wire-Wrapped Assemblies," Trans. of the American Nuclear Society, Vol. 30, pp 547-548 (1978).

M. Fakory and N. Todreas, "Experimental Investigation of Flow Resistance and Wall Shear Stress in the Interior Subchannel of a Triangular Array of Parallel Rods," Jl. Fluids Eng., Vol. 101, pp 429-435 (Dec. 1979).

J. G. Bartzis and N. E. Todreas, "Turbulence Modeling of Axial Flow in a Bare Rod Bundle," Jl. Ht. Trans., Vol. 101, No. 4, pp 628-634 (Nov. 1979).

Reports Issued Under This Contract

C. Papers and Summaries (Continued)

C. Chiu, W. M. Rohsenow, and N. E. Todreas, "Prediction of Temperature Distribution in Wire-Wrapped Nuclear Fuel Rod Assemblies," Proceedings NATO Mtg, Vol. 1, pp 175-184, published by Hemisphere Pub. Co., Washington, DC (1978).

S. Glazer, T. Greene, N. Todreas, and L. Wolf, "Transient Thermal-Hydraulic Analysis in the Forced-Convection Regime (TRANSENERGY)," TANSOA, Vol. 32, Atlanta, 1979.

C. Chiu, W. M. Rohsenow, and N. E. Todreas, "Turbulent Flow Split Model and Supporting Experiments for Wire-Wrapped Core Assemblies," Nuclear Technology, Vol. 50, pp 40-52, August 1980.

Chiu, C., Hawley, J. T., Rohsenow, W. M., and Todreas, N. E., "Parameters for Laminar, Transition and Turbulent Longitudinal Flows in Wire Wrap Spaced Hexagonal Arrays," Accepted for presentation at the Topical Meeting on Nuclear Reactor Thermal Hydraulics, Saratoga, NY, October 5-8, 1980.

Rohsenow, W. M., Todreas, N. E., Wang, S. F., "Buoyancy Effects on Subchannel Friction Factors in Bare Rod Bundles," Submitted for consideration at Specialists' Meeting on Decay Heat Removal and Natural Convection in FBRs," February 28-29, 1980, Upton, New York.

Chiu, C., Morris, R., and N. Todreas, "Experimental Techniques for Liquid Metal Cooled Fast Breeder Reactor Fuel Assembly Thermal/Hydraulic Tests," Invited Paper for Special Issue of Nuclear Engineering and Design ,Vol.62,No.1-3, 253-270,Dec.1980.

Bishop, A. and N. Todreas, "Hydraulic Characteristics of Wire-Wrapped Rod Bundles," Invited Paper for Special Issue of Nuclear Engineering and Design, Vol.62,No.1-3, 271-293,Dec.1980.

ABSTRACT

This report provides a current summary of recommended values of key input parameters required for ENERGY code analysis of LMFBR wire wrapped bundles. This data is based on the interpretation of experimental results from the MIT and other available laboratory programs.

REVISION RECORD

Revision 1 was prepared based principally on the efforts of Kerry Basehore and Chong Chiu. Kerry was instrumental in clarifying the difference between continuum and subchannel notation and Chong is responsible for producing the new flow split and mixing parameter correlations. Thanks are also due to Mike Corradini who has labored through the preparation of Chong's reports and this one to ensure the clarity and accuracy.

Revision 2 was initiated by James Hawley and was completed by Yee-Ning Chan. The latter made a great effort to reduce typographical and transformation errors and to ensure that the nomenclatures and definitions are accurate and consistent both throughout the report and with other reports released by the LMFBR research group of the Massachusetts Institute of Technology. A new Chapter 3 on friction factors has been added and Chapter 5 has been expanded to include a section on the Energy Code Parameters for laminar flow. Figures 1 and 2 were replotted because the original figures were found to be inaccurate.

The definition of ∇h was changed from h_i-h_j/η to h_j-h_i/η in the Nomenclature. Consequently, the "-" signs preceding the turbulent diffusion terms were all changed to "+" signs in the text.

NOMENCLATURE

Representation (Continuum or Subchannel) → P^{Ψ}

- Ψ: * → Normalized or Dimensionless (* or Blank)
- Ψ: A,I → Bundle region (I, II or Blank for overall Bundle) or Subchannel type (1, 2 or 3)
- Ψ: Orientation (Axial, Normal or Swirl)

CONTINUUM	SUBCHANNEL
Velocities	
U_A	$V_A = U_A \left(\frac{1}{\lambda_A}\right)$
U_{A_I}	$V_{A_I} = U_{A_I}\left(\frac{1}{\lambda_{A_I}}\right)$
$U_{A_{II}}$	$V_{A_{II}} = U_{A_2}\left(\frac{1}{\lambda_{A_{II}}}\right)$
$U_{S_{II}}$	$V_{S_{II}} = U_{S_2}\left(\frac{1}{\lambda_{L_{II}}}\right)$
Volumetric Heat Sources	
P^Q	$S^Q = P^Q \left(\frac{1}{\lambda_A}\right)$
P^{Q_I}	$S^{Q_I} = P^{Q_I}\left(\frac{1}{\lambda_{A_I}}\right)$
$P^{Q^*_I} = \frac{P^{Q_I}}{P^Q}$	$S^{Q^*_I} = P^{Q^*_I}\left(\frac{\lambda_A}{\lambda_{A_I}}\right)$
$P^{Q_{II}}$	$S^{Q_{II}} = P^{Q_{II}}\left(\frac{1}{\lambda_{A_{II}}}\right)$
$P^{Q^*_{II}} = \frac{P^{Q_{II}}}{P^Q}$	$S^{Q^*_{II}} = P^{Q^*_{II}}\left(\frac{\lambda_A}{\lambda_{A_{II}}}\right)$
Flow Splits	
$P^{X_I} = P^{X_1} = \frac{U_{A_I}}{U_A} = \frac{U_{A_1}}{U_A}$	$S^{X_I} = S^{X_1} = \frac{\lambda_A}{\lambda_{A_I}} P^{X_I} = \frac{V_{AI}}{V_A}$
$P^{X_{II}} = \frac{U_{A_{II}}}{U_A}$	$S^{X_{II}} = \frac{\lambda_A}{\lambda_{A_{II}}} P^{X_{II}} = \frac{V_{AII}}{V_A}$
$P^{X_2} = \frac{U_{A2}}{U_A}$	$S^{X_2} = \frac{\lambda_A}{\lambda_{A_2}} P^{X_2} = \frac{V_{A2}}{V_A}$
Shape FACTORS	
P^K_{NI}	$S^K_{NI} = \frac{P^K_{NI}}{\lambda_{LI}}$
$P^K_{NII} = pK_{NI}$	$S^K_{NII} = \frac{P^K_{NII}}{\lambda_{LI}} \equiv S^K_{NI}$
P^K_{SII}	$S^K_{SII} = \frac{P^K_{SII}}{\lambda_{LII}}$

Perimeter for Heat Transfer

$$ {}_{P}\mathbb{P}_{I} \qquad {}_{S}\mathbb{P}_{I} = \lambda_{LI}\ {}_{P}\mathbb{P}_{I} $$

$$ {}_{P}\mathbb{P}_{SII} \qquad {}_{S}\mathbb{P}_{SII} = \lambda_{LII}\ {}_{P}\mathbb{P}_{SII} $$

$$ {}_{P}\mathbb{P}_{NII}\ (\equiv {}_{P}\mathbb{P}_{I}) \qquad {}_{S}\mathbb{P}_{NII} = \lambda_{NII}\ {}_{P}\mathbb{P}_{NII} \equiv \lambda_{LI}\ {}_{P}\mathbb{P}_{I} = {}_{S}\mathbb{P}_{I} $$

Cross-Sectional Area for Flow

$$ {}_{P}A_{I} \qquad {}_{S}A_{I} = \lambda_{AI}\ {}_{P}A_{I} $$

$$ {}_{P}A_{II} \qquad {}_{S}A_{II} = \lambda_{AII}\ {}_{P}A_{II} $$

Key parameters which are the same for continuum and subchannel models

Enthalpy $$ h_{I \text{ or } II} = C_p\ T_{I \text{ or } II} $$

$$ h^* = \frac{\rho C_p\ T\ U_A}{{}_{P}Q\ D_{e_l}} = \frac{\rho C_p\ T\ V_A}{{}_{S}Q\ D_{e_l}} $$

Axial Mass Flow Rate

$$ m_A = \rho\ {}_{P}A\ U_A = \rho\ {}_{S}A\ V_A $$

Gradient

$$ \nabla h = \frac{h_j - h_i}{\eta} $$

$$ \nabla^* h = \frac{h_j^* - h_i^*}{\eta / D_{e_l}} $$

ADDITIONAL NOMENCLATURE NOT FOLLOWING THE PREVIOUS CONVECTION

C, C_1, C_L, C_{1L}	Swirl velocity parameters - see TABLE 2
$\varepsilon^*, \varepsilon_1^*, \varepsilon_L^*, \varepsilon_{1L}^*$	Mixing parameters - see TABLE 2
$\alpha^*, \alpha_1^*, \alpha_{II}^*, \alpha_L^*, \alpha_{1L}^*$	Conduction parameters - see TABLE 3
$\varepsilon_{H_{NI}}, \varepsilon_{H_{NII}}, \varepsilon_{H_{SII}}$	Directional eddy diffusivities - see TABLE 3 appearing directly in continuum equations.
$\lambda_A, \lambda_{AI}, \lambda_{AII}, \lambda_{LI}, \lambda_{LII}$	Porosity factors - see TABLE 1
A_r	Projected area of wires in subchannel m^2 (ft^2)
A_{r_1}	Projected area of wires in interior subchannel m^2 (ft^2)
A_{r_2}	Projected area of wires in edge subchannel m^2 (ft^2)
A_{s_1}	Axial average interior subchannel area for a wire-wrapped rod bundle m^2 (ft^2)
A_{s_2}	Axial average edge subchannel area for a wire-wrapped rod bundle m^2 (ft^2)
A_{s_3}	Axial average corner subchannel area for a wire-wrapped rod bundle m^2 (ft^2)
A_s'	Subchannel area for a bare rod bundle, m^2 (ft^2)
A_{s_1}'	Interior subchannel area for a bare rod bundle, m^2 (ft^2)
A_{s_2}'	Edge subchannel area for a bare rod bundle, m^2 (ft^2)
D_e	Overall hydraulic diameter, m (ft)
D_{e_1}	Equivalent hydraulic diameter for interior subchannels of a wire-wrapped bundle, m (ft) (superscript ' for bare rod bundle)

D_{e_2}	Equivalent hydraulic diameter for edge subchannels of a wire-wrapped bundle, m (ft) (superscript ' for bare-rod bundle)
D_F	Distance across flats of a hexagon, m (ft)
D	Rod diameter, m (ft)
D_g	Distance between rod and duct wall, m (ft)
D_w	Wire diameter, m (ft)
F	Looseness factor
Gap	Gap between interior subchannels, m (ft)
H	Wire wrap lead length, m (ft)
N_1	Number of interior subchannels in the bundle
N_2	Number of edge subchannels in the bundle
N_3	Number of corner subchannels in the bundle
n	Ratio of the gap between edge subchannels to the average edge subchannel width
N_p	Number of fuel pins in assembly
N_{RINGS}	Number of rings of rods in an array. The center pin itself is ring number 0
P	Fuel pin pitch
T_{ff}	Flat-to-flat tolerance, m(ft)
V_T	Average transverse velocity i.e., V_{SII}

TABLE OF CONTENTS

		Page
ABSTRACT		xiii
REVISION RECORD		xiv
NOMENCLATURE		xv
TABLE OF CONTENTS		xix
LIST OF FIGURES		xx
LIST OF TABLES		xx
CHAPTER 1.0	INTRODUCTION	1
CHAPTER 2.0	INPUT PARAMETER DEFINITIONS	2
2.1	Inner Bundle Region	3
2.2	Outer Bundle Region	8
2.3	Porosity Factors	14
2.4	Conversions Among Mixing and Swirl Parameters	16
CHAPTER 3.0	FRICTION FACTORS	18
3.1	Laminar Flow Correlations for f_1 and f_2	18
3.2	Turbulent Flow Correlations for f_1 and f_2	19
3.3	Transition Flow Correlations for f_1 and f_2	20
3.4	Bundle Friction Factors	20
3.5	Important User's Note	20
CHAPTER 4.0	FLOW SPLIT	21
4.1	Region and Subchannel Flow Splits	21
4.2	Correlations for x_2 and x_2	22
4.3	Effect of Tolerances	24
4.4	Important User's Note	24
CHAPTER 5.0	WIRE SWEEPING CORRELATIONS	25
5.1	ENERGY Code Parameters, Turbulent Flow	27
5.2	ENERGY Code Parameters, Laminar Flow	29
CHAPTER 6.0	CRITERION TO DETERMINE WHEN BUOYANCY EFFECTS ARE IMPORTANT	30a
6.1	Skewed Radial Power Profile	30a
6.2	Flat Radial Power Profile	31
CHAPTER 7.0	IMPORTANT NOTE ON ENERGY CODE LISTING	36
REFERENCES		37
FIGURES		39
TABLES		51

LIST OF FIGURES

Figure		Page
1	Percent Change in $\frac{\lambda_A}{\lambda_{L1}}$ as a Function of $\frac{P}{D}$, $\frac{H}{D}$ and N with respect to $\frac{H}{D} = 16$.	39
2	Porosity Ratio for ε_1^* to ε^* Conversion.	40
3	Porosity Ratio for C_1 to C Conversion	41
4	Parameter n in Eqn. (45) versus $\frac{P}{D}$ Ratio.	42
5	Ratio of Flow Splits for Region II and Edge Subchannels.	43
6	Predicted Interior Flow Split Parameter X_1.	44
7	Predicted Edge Flow Split Parameter X_2.	45
8	Definition of Flat Tolerance and Rod Alignment Modes of F = 1 and F = 0.	46
9	Comparison Between Original and New Correlations for ε^*_{1L}.	47
10	Comparison Between Original and New Correlations for for C_{1L}.	48
11	ε^*_{1L} Predicted Behavior.	49
12	C_{1L} Predicted Behavior.	50

LIST OF TABLES

Table		Page
I	Porosity Factors	51
II	Parameters for Turbulent Bundle Analysis	52
III	Complete Table of Parameters for Bundles Analysis	53

1.0 INTRODUCTION

The purpose of this report is to provide an updated summary of recommended values of input data required by analysts for hexagonal wire wrapped bundles. This data is based on the interpretation of experimental results from the MIT and other available laboratory programs. The input data has been expressed specifically in the forms used in the ENERGY code family. It is intended that this report will be updated as data analysis yields (1) new input data for rod bundle geometries already surveyed or (2) input data for new rod bundle geometries.

The ENERGY family was originally formulated in both continuum and subchannel representation (1, 2 and 3).* The continuum formulation reflected the physical model underlying our method of approach and gives great flexibility in the range of problems to which the model can be applied. The subchannel representation is simply a special case of the porous body formulation in which the relevant parameters are established on a subchannel basis for user's ease in application of our model to this common way of discretizing a bundle. Our decision to retain both representations has resulted in some confusion regarding the proper form of the input parameters for each case due to (1) the complexity of the notation and (2) typographical and transformation errors in some of our own publications.

Because of the range of potential applications, we choose to retain both representations and strive to overcome the notational difficulties by a lucid presentation of definitions of parameters. The parameter definitions are presented in the next chapter and are followed by the recommended correlations for these parameters.

The correlations are based on physical models which should permit their extrapolation to some degree outside the range of the data base used in their development.

$$4 \leqslant H/D \leqslant 52$$

$$1.067 \leqslant P/D \leqslant 1.32$$

The bundles must have all wire wraps of the same diameter, wrapped in the same orientation from the same start position.

---

*Here we originally called our representations "porous body" and "subchannel". It is more proper to call them continuum and subchannel where the subchannel is a special case of a porous body representation.

2.0 INPUT PARAMETER DEFINITIONS

The parameter definitions and their interrelationships are best presented in terms of the governing differential equations. For the ENERGY model these are the energy transport equations in the inner (region I) and outer (region II) regions of the bundle. Usually nomenclature is completely relegated to a table but we shall present our approach here now because it is complicated by our desire to present both the continuum and the subchannel approaches on a consistent basis. Let ψ represent any variable. Then

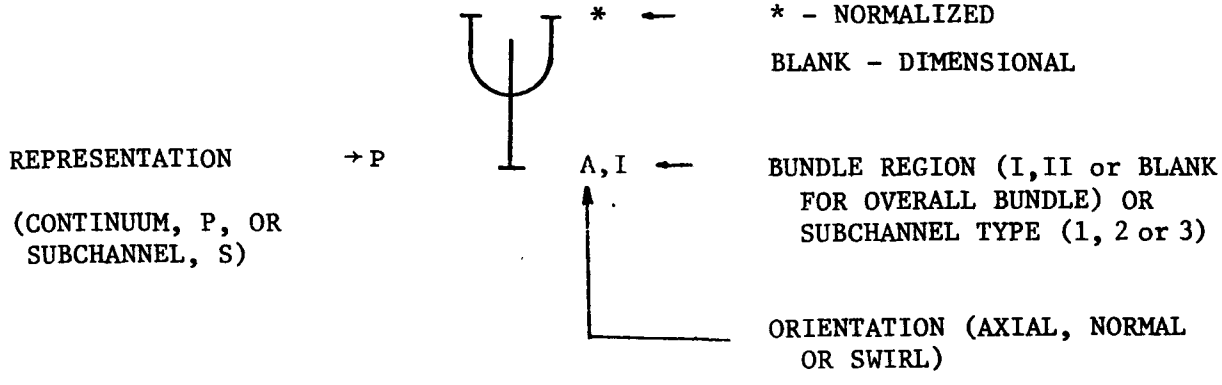

The key exceptions to the above convention include:

Velocities where instead of P or S we change ψ from U for continuum to V for subchannel.

Porosities λ where the * is dropped since by definition they are dimensionless and L is used for the lateral or N for normal direction

Subchannel areas where the orientation is dropped because they are all axial

2.1 INNER BUNDLE REGION

2.11 Continuum Representation (ε^*)

In a continuum representation the choice of the control volume shape is at the user's discretion. In this application the control volume chosen for region I is an equilateral triangular prism, Δz units in length, which from physical considerations comprises the planar area of at least one subchannel and the sixth sector of each of three rods which border the subchannel i.e.

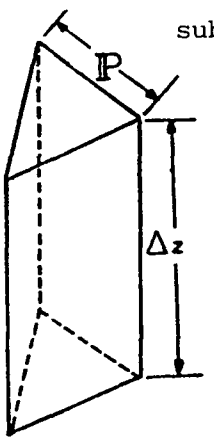

REGION I
CONTROL VOLUME
(for a planar area of one subchannel, the perimeter **P** numerically is equal to the pitch P.)

The energy transport equation for this control volume in our continuum representation is

$$ {}_{P}A_{I}\ \rho C_{P}\ U_{AI}\ (T_{OUT} - T_{IN}) = (\rho C_{P}\ \epsilon_{H_{NI}} + {}_{P}K_{NI}\ K)\ {}_{P}P_{I}\ \Delta z\ \nabla T + {}_{P}Q_{I}\Delta z\ {}_{P}A_{I} \qquad (1\ a) $$

$$ \text{or} \qquad \rho U_{AI}\ \frac{\partial h}{\partial z} = \left(\frac{P}{A}\right)_{I}\ \rho(\epsilon_{H_{NI}} + {}_{P}K_{NI}\alpha)\ \nabla h + {}_{P}Q_{I} \qquad (1\ b) $$

where the effective conduction term with the enthalpy gradient is taken across each of the three lateral faces of the control volume.

We next bring equation (1 b) into dimensionless form utilizing the parameters U_A, D_{e_I}, and ${}_{P}Q$. The first two parameters are selected because they are convenient and unambiguous parameters. It may seem strange to adopt D_{e_I} since it is a subchannel parameter but recall that in the continuum model, the only characteristic dimensions available are those of the duct or the actual subchannels since the node size is arbitrary.

Utilizing these parameters, equation (1 b) becomes

$$\frac{U_{AI}}{U_A}\,\frac{\partial(h\,\rho\,U_A/P^Q\,D_{e_1})}{\partial(z/D_{e_1})} = D_{e_1}\,\left(\frac{\mathbb{P}}{A}\right)_{P\ I}\left(\frac{\epsilon_{H_{NI}}}{U_A\,D_{e_1}} + P\,K_{NI}\,\frac{\alpha}{U_A\,D_{e_1}}\right)\frac{\nabla(h\rho\,U_A/P^Q\,D_{e_1})}{1/D_{e_1}} + \frac{P^Q{}_I}{P^Q} \qquad (2)$$

$$\text{or}\quad \frac{U_{AI}}{U_A}\,\frac{\partial h^*}{\partial z^*} = D_{e_1}\,\left(\frac{\mathbb{P}}{A}\right)_{P\ I}\left(\epsilon^* + P\,K_{NI}\,\alpha^*\right)\nabla^* h + P^Q{}^*_I \qquad (3)$$

which defines the continuum parameters ϵ^* and α^*

$$\epsilon^* \equiv \frac{\epsilon_{H_{NI}}}{U_A\,D_{e_1}} \quad \text{and} \quad \alpha^* \equiv \frac{\alpha}{U_A\,D_{e_1}} \qquad (4\ a,b)$$

2.1.2 Subchannel Representations (ϵ^*_1, ϵ^*_{1L})

Now for convenience a subchannel based representation is desired in which all parameters appearing in the energy equation are the true values in the rod array. Hence we transform equation (3) into that form by introducing lateral and axial porosity factors defined in Table I. Note that the lateral porosity between interior rods is taken to be the ratio of the gap between rods to the pitch to be consistent with the change in the perimeter P for heat flow, i.e., P-D versus P. For the outer region the same convention is adopted i.e., taking the gap between rod surface, D_g, and duct as the relevant dimension.

Applying porosity factors to equation (3), we obtain :

$$\frac{\lambda_{A_I}}{\lambda_A}\left(\frac{U_{AI}/\lambda_{AI}}{U_A/\lambda_A}\right)\frac{\partial h^*}{\partial z^*} = \frac{\lambda_{LI}\,D_{e_1}}{\lambda_{AI}}\,P\left(\frac{\mathbb{P}}{A}\right)_I\left(\frac{\lambda_{AI}\,\epsilon^*}{\lambda_{LI}} + \frac{\lambda_{AI}}{\lambda_{LI}}\,P\,K_{NI}\,\alpha^*\right)\nabla^* h + P^Q{}^*_I\,\frac{\lambda_{AI}}{\lambda_{AI}} \qquad (5)$$

Now the following relations exist between continuum and subchannel parameters :

$$\lambda_{LI}\ {}_{P}\mathbb{P}_{I} = {}_{S}\mathbb{P}_{I} \tag{6 a}$$

$$\lambda_{AI}\ {}_{P}A_{I} = {}_{S}A_{I} \tag{6 b}$$

$$\left(\frac{\lambda_A}{\lambda_{AI}}\right)\ {}_{P}Q^{*}_{I} = \frac{{}_{P}Q_{I}/\lambda_{AI}}{{}_{P}Q/\lambda_{A}} = {}_{S}Q^{*}_{I} \tag{6 c}$$

$$\frac{U_{AI}/\lambda_{AI}}{U_{A}/\lambda_{A}} = \frac{V_{AI}}{V_{A}} = {}_{S}X_{I} = {}_{S}X_{1} \tag{6 d}$$

Note that in the last relation we have introduced the definitions for flow split in the subchannel representation and since region I is comprised exclusively of interior subchannel (type 1) we note that ${}_{S}X_{I}={}_{S}X_{1}$ and that ${}_{S}A_{I}=A_{S1}$.

Utilizing these relations equation (5) becomes :

$${}_{S}X_{1}\frac{\partial h^{*}}{\partial z^{*}} = {}_{De_1}\ {}_{S}\left(\frac{\mathbb{P}}{A}\right)_{I}\left(\frac{\lambda_A\,\epsilon^{*}}{\lambda_{LI}} + \frac{\lambda_A}{\lambda_{LI}}\,{}_{P}K_{NI}\,\alpha^{*}\right)\nabla^{*}h + {}_{S}Q^{*}_{I}$$

$$\text{or}\quad {}_{S}X_{1}\frac{\partial h^{*}}{\partial z^{*}} = {}_{De_1}\left(\frac{\mathbb{P}}{A}\right)_{I}\ (\epsilon^{*}_{1} + {}_{S}K_{NI}\,\alpha^{*}_{1})\ \nabla^{*}h + {}_{S}Q^{*}_{I} \tag{7}$$

This is the origin of the subchannel based parameters ϵ^{*}_{1} and α^{*}_{1}

$$\text{i.e.}\quad \epsilon^{*}_{1} = \frac{\lambda_A}{\lambda_{LI}}\,\epsilon^{*}\ ;\ \alpha^{*}_{1} = \lambda_A\,\alpha^{*}\ \text{and}\ {}_{S}K_{NI} = \frac{{}_{P}K_{NI}}{\lambda_{LI}} \tag{8 a, b, c}$$

The application of porosity factors λ_A and λ_{LI} in equations 8 b and 8 c follows physically since α^{*} includes an axial velocity and ${}_{P}K_{NI}$ is a correction factor for lateral heat transfer. Note also that in previous reports the factor ${}_{S}K_{NI}$ was called "SF".

Analysis of LMFBR assemblies is based on equation (3) or (7) with parameters ϵ^{*} or ϵ^{*}_{1}, α^{*} or α^{*}_{1}, and ${}_{P}K_{NI}$ or ${}_{S}K_{NI}$ as input. The parameters ϵ^{*} and ϵ^{*}_{1} are determined from reduction of either heated pin bundle or

salt injection test data by the inverse use of equation (3) or (7). In this inverse use, the enthalpy or analogously the salt concentration, are known, α^* or α^*_l and $K_{P\,NI}$ or $K_{S\,NI}$ are input and ϵ^* or ϵ^*_l is determined by trial and error. From equations (3) or (7) we see that the resulting value of ϵ^* or ϵ^*_l is dependent on the flow split ($\frac{U_{AI}}{U_A}$ for continuum, $\frac{V_{AI}}{V_A}$ for subchannel) which is equivalent to saying they are functions of bundle size. This dependance of the interior region mixing parameter can be eliminated by redefinition of the parameter to incorporate the flow split. We will show this explicitly for the subchannel formulation by dividing equation (7) by $_SX_l$ yielding

$$\frac{\partial h^*}{\partial z^*} = De_l \left(\frac{P}{A}\right)_I \left(\frac{\lambda_A \epsilon^*}{{}_SX_l\ \lambda_{LI}} + K_{P\,NI}\ \frac{\lambda_A \alpha^*}{\lambda_{LI}\ {}_SX_l}\right) \nabla^* h + \frac{{}_SQ^*_I}{{}_SX_l}$$

$$\text{or}\quad \frac{\partial h^*}{\partial z^*} = De_l \left(\frac{P}{A}\right)_I \left(\epsilon^*_{lL} + K_{S\,NI}\ \alpha^*_{lL}\right) \nabla^* h + \frac{{}_SQ^*_I}{{}_SX_l} \qquad (9)$$

where :

$$\epsilon^*_{lL} = \frac{1}{{}_SX_l}\ \frac{\lambda_A}{\lambda_{LI}}\ \epsilon^* = \frac{\epsilon^*_l}{{}_SX_l}\ ;\ \alpha^*_{lL} = \lambda_A \alpha^* = \frac{\alpha^*_l}{{}_SX_l}\ \text{ and again }\ K_{S\,NI} = \frac{K_{P\,NI}}{\lambda_{LI}}$$

(10 a, b and 8 c)

For salt conductivity experiments the salt is input only at one plane and hence appears only as a boundary condition when salt data is used in the concentration equation analogous to (9) to deduce ϵ^*_{lL}. There is no source term. Therefore the deduced values of ϵ^*_{lL} are independent of bundle size i.e. $_SX_l$ for highly turbulent flow where $\epsilon^*_{lL} >> {}_SK_{NI}\ \alpha^*_{lL}$. On the other hand, for heated bundle data reduction by equation (9), knowledge of $_SX_l$ is necessary to obtain the proper value of ϵ^*_{lL}. To use equation (9) for assembly temperature field prediction, accurate knowledge of $_SX_l$ is also needed to correctly express the source term. Therefore we formulate the results of salt mixing tests in terms of ϵ^*_{lL} to be independent of bundle size and we independently perform experiments to determine $_SX_l$.

2.1.3 Continuum Representation (ε^*_L)

To complete this discussion and illustrate the symmetry of our definitions we observe that the continuum mixing coefficient, independent of bundle size, can be obtained by dividing equation (3) by $\frac{U_{AI}}{U_A}$ which from equation (6d) and the definition for flow split from the continuum model is

$$\frac{U_{AI}}{U_A} = {}_S X_1 \frac{\lambda_{AI}}{\lambda_A} \equiv {}_P X_1 \equiv {}_P X_I \tag{11}$$

yielding

$$\frac{\partial h^*}{\partial z^*} = De_1 \left(\frac{\mathbb{P}}{A}\right)_I \left(\frac{\epsilon^*}{{}_P X_1} + {}_P K_{NI} \frac{\alpha^*}{{}_P X_1} \right) \nabla^* h + \frac{{}_P Q^*_I}{{}_P X_1}$$

or

$$\frac{\partial h^*}{\partial z^*} = De_1 \left(\frac{\mathbb{P}}{A}\right)_I (\epsilon^*_L + {}_P K_{NI} \alpha^*_L) \nabla^* h + \frac{{}_P Q^*_I}{{}_P X_1} \tag{12}$$

where $\epsilon^*_L = \left(\frac{1}{{}_S X_1} \frac{\lambda_A}{\lambda_{AI}} \right) \epsilon^* = \frac{\epsilon^*}{{}_P X_1}$ and $\alpha^*_L = \left(\frac{1}{{}_S X_1} \frac{\lambda_A}{\lambda_{AI}} \right) \alpha^* = \frac{\alpha^*}{{}_P X_1}$

(13a, b)

2.1.4 Summary of Inner Region Relations

The resulting forms of the mixing coefficients for the four representations, equations 4a, 8a, 10a and 13a are listed in Table 2. One can note that symmetry does not exist in passing from bundle size dependent parameters to the corresponding bundle size independent cases. Specifically, the parameters for the continuum formulations are related as

$$\varepsilon^*_L = \frac{\varepsilon^*}{{}_S X_1} \left(\frac{\lambda_A}{\lambda_{AI}}\right)$$

where as the subchannel formulations are related as

$$\varepsilon^*_{1L} = \frac{\varepsilon^*_1}{{}_S X_1}$$

This difference occurs because the subchannel based flow split ${}_S X_1$ is used in both cases. The ratio $\frac{\lambda_A}{\lambda_{AI}}$ could be eliminated if a continuum based flow split was used. However, since experimentally determined flow splits are based on subchannel velocity ratios, we have chosen to use ${}_S X_1$ throughout and accept the resulting lack of symmetry in definitions.

2.2 OUTER BUNDLE REGION

2.2.1 Continuum Representation (C)

The energy transport equation for region II in the continuum representation may be written as

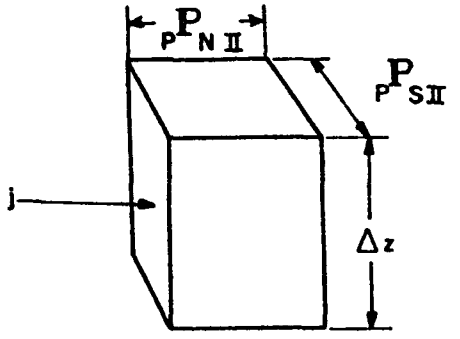

REGION II
CONTROL VOLUME

Where $_{P}\mathbb{P}_{N_{II}} = P$

$_{P}\mathbb{P}_{S_{II}} = \frac{D}{2} + D_g$

$$\rho C_P\, U_{S\,II}\, {}_{P}\mathbb{P}_{S\,II}\, \Delta z\, (T_i - T_j) + \rho C_P\, U_{A\,II}\, {}_{P}A_{II}\, (T_{OUT} - T_{IN})$$

$$= (\rho C_P \epsilon_{H_{NII}} + {}_{P}K_{NII} K)\, {}_{P}\mathbb{P}_{NII}\, \Delta z\, \nabla T$$

$$+ (\rho C_P \epsilon_{H_{SII}} + {}_{P}K_{SII} K)\, {}_{P}\mathbb{P}_{SII}\, \Delta z\, \nabla T + {}_{P}Q_{II}\, \Delta z\, {}_{P}A_{II} \qquad (14a)$$

$$\text{or}\quad \rho U_{S\,II} \left(\frac{{}_{P}\mathbb{P}_{S\,II}\; {}_{P}\mathbb{P}_{N\,II}}{{}_{P}A_{II}} \right) \frac{\partial h}{\partial s} + \rho U_{A\,II} \frac{\partial h}{\partial z}$$

$$= \left(\frac{{}_{P}\mathbb{P}_{N\,II}}{{}_{P}A_{II}} \right) \rho\, (\epsilon_{H_{NII}} + {}_{P}K_{NII}\alpha)\, \nabla h$$

$$+ \left(\frac{{}_{P}\mathbb{P}_{S\,II}}{{}_{P}A_{II}} \right) \rho\, (\epsilon_{H_{SII}} + {}_{P}K_{SII}\alpha)\, \nabla h + {}_{P}Q_{II} \qquad (14b)$$

Bringing the equation into dimensionless form utilizing again the parameters U_A, De_1 and ${}_{P}Q$, we obtain:

$$\frac{U_{SII}}{U_A}\left(\frac{P\mathbb{P}_{SII}\ P\mathbb{P}_{NII}}{P^A_{II}}\right)\frac{\partial(\rho h\ U_A/P^Q\ D_{e_1})}{\partial(S/D_{e_1})}+\frac{U_{AII}}{U_A}\frac{\partial(\rho h\ U_A/P^Q\ D_{e_1})}{\partial(Z/D_{e_1})}=\frac{P^Q_{II}}{P^Q}$$

$$D_{e_1}\left(\frac{P\mathbb{P}_{NII}}{P^A_{II}}\right)\left(\frac{\epsilon_{H_{NII}}}{U_A\ D_{e_1}}+\frac{K}{P_{NII}}\frac{\alpha}{U_A\ D_{e_1}}\right)\frac{\nabla(\rho h\ U_A/P^Q\ D_{e_1})}{1/D_{e_1}}$$

$$+\quad D_{e_1}\left(\frac{P\mathbb{P}_{SII}}{P^A_{II}}\right)\left(\frac{\epsilon_{H_{SII}}}{U_A\ D_{e_1}}+\frac{K}{P_{SII}}\frac{\alpha}{U_A\ D_{e_1}}\right)\frac{\nabla(\rho h\ U_A/P^Q\ D_{e_1})}{1/D_{e_1}} \qquad (15)$$

At this point rather than defining various directionally and region dependent mixing parameters, we note that (1) the diffusivity effects of the RHS for turbulent flow and probably to some as yet unconfirmed level of laminar flow are much smaller than the convective effects (1^{st} term LHS) and (2) the diffusivity effects are approximately equal for all regions in all directions of the bundle. Therefore take the eddy diffusivity as isotropic, yielding

$$\epsilon^* \equiv \frac{\epsilon_{H_{NII}}}{U_A\ D_{e_1}} \cong \frac{\epsilon_{H_{SII}}}{U_A\ D_{e_1}} \cong \frac{\epsilon_{H_{NI}}}{U_A\ D_{e_1}} \qquad (16)$$

In a consistent manner the molecular conduction could be approximated as equal in cases where conduction effects are not significant. However we will retain the regional and directional notation for generality.

Expressing equation (15) in dimensionless nomenclature we have :

$$C\left(\frac{P\mathbb{P}_{SII}\ P\mathbb{P}_{NII}}{P^A_{II}}\right)\frac{\partial h^*}{\partial S^*}+\frac{U_{AII}}{U_A}\frac{\partial h^*}{\partial Z^*}= D_{e_1}\left(\frac{P\mathbb{P}_{NII}}{P^A_{II}}\right)(\epsilon^*+\frac{K}{P_{NII}}\alpha^*)\nabla^* h$$

$$+\quad D_{e_1}\left(\frac{P\mathbb{P}_{SII}}{P^A_{II}}\right)(\epsilon^*+\frac{K}{P_{SII}}\alpha^*)\nabla^* h$$

$$+\ P^{Q^*}_{II} \qquad (17)$$

Note that we have introduced a new parameter, the swirl velocity ratio as

$$C = \frac{U_{SII}}{U_A} \qquad (18)$$

2.2.2 Subchannel Representation (C_1, C_{1L})

Proceeding to a subchannel representation we transform equation (17) to the following form by introducing porosity factors

$$\left(\frac{{}_P\mathbb{P}_{SII}\ {}_P\mathbb{P}_{NII}}{P^A_{II}}\right)\frac{\lambda_{LII}}{\lambda_A}\left(\frac{U_{SII}/\lambda_{LII}}{U_A/\lambda_A}\right)\frac{\partial h^*}{\partial s^*}+\frac{\lambda_{AII}}{\lambda_A}\left(\frac{U_{AII}/\lambda_{AII}}{U_A/\lambda_A}\right)\frac{\partial h^*}{\partial z^*}=$$

$$De_1\left(\frac{{}_P\mathbb{P}_{NII}}{P^A_{II}}\right)\frac{\lambda_{LI}}{\lambda_{AII}}\left(\frac{\lambda_{AII}\,\epsilon^*}{\lambda_{LI}}+\frac{\mathbb{K}}{{}_P\mathbb{P}_{NII}}\,\lambda_{AII}\,\alpha^*\right)\nabla^*_h$$

$$+\quad De_1\left(\frac{{}_P\mathbb{P}_{SII}}{P^A_{II}}\right)\frac{\lambda_{LII}}{\lambda_{AII}}\left(\frac{\lambda_{AII}\,\epsilon^*}{\lambda_{LII}}+\frac{\mathbb{K}}{{}_P\mathbb{P}_{SII}}\,\lambda_{AII}\,\alpha^*\right)\nabla^*_h\ +\ {}_PQ^*_{II}\,\frac{\lambda_{AII}}{\lambda_{AII}}\qquad(19)$$

Next we introduce the subchannel flow split definition for the outer region

$$S^X_{II}=\frac{V_{AII}}{V_A}=\frac{U_{AII}/\lambda_{AII}}{U_A/\lambda_A}\qquad(20a)$$

(Note that this flow split definition is based on the condition in the entire outer region which includes both edge and corner channels. In our experimental reports we have separately identified the flow split in each of the three subchannel types as 1 - interior, 2 - edge, and 3 - corner. Therefore X_{II} is not strictly equal to X_2 because of the presence of corner channels in region II and we have introduced the notation X_{II} to highlight this difference. In practical cases for large rod bundles, 37 pins or greater, X_{II} can be taken equal to X_2).

Also we note the following relations between continuum and subchannel parameters

$$\lambda_{AII}\ {}_PA^A_{II}={}_SA^A_{II}\qquad(20b)$$

$$\lambda_{LII}\ {}_P\mathbb{P}_{SII}={}_S\mathbb{P}_{SII}\qquad(20c)$$

$$\lambda_{LI}\ {}_P\mathbb{P}_{NII}={}_S\mathbb{P}_{NII}={}_S\mathbb{P}_I\qquad(20d)$$

$$(\text{since }\lambda_{LI}\equiv\lambda_{NII}\text{ and }{}_P\mathbb{P}_{NII}\equiv{}_P\mathbb{P}_I)$$

$$\left(\frac{\lambda_A}{\lambda_{AII}}\right) {}^{P}Q^{*}_{II} = \frac{{}^{P}Q_{II}/\lambda_{AII}}{{}^{P}Q/\lambda_A} = {}^{S}Q^{*}_{II} \qquad (20\ e)$$

Applying relations (20 a) thru (20 e) to equation (19), we obtain :

$$\left(\frac{{}^{\mathbb{P}}S_{II}\ {}^{P}\mathbb{P}_{NII}}{{}^{S}A_{II}}\right) C_1 \frac{\partial h^*}{\partial s^*} + {}^{S}X_{II} \frac{\partial h^*}{\partial z^*}$$

$$= D_{e_1}\left(\frac{{}^{S}\mathbb{P}_{NII}}{{}^{S}A_{II}}\right)\left(\frac{\lambda_A}{\lambda_{LI}}\epsilon^* + \frac{{}^{P}K_{NII}}{\lambda_{LI}}\lambda_A\alpha^*\right)\nabla^* h \qquad (21)$$

$$+ D_{e_1}\left(\frac{{}^{S}\mathbb{P}_{SII}}{{}^{S}A_{II}}\right)\left(\frac{\lambda_A\epsilon^*}{\lambda_{LII}} + \frac{{}^{P}K_{SII}}{\lambda_{LII}}\lambda_A\alpha^*\right)\nabla^* h + {}^{S}Q^{*}_{II}$$

Finally we usually make the simplification that

$$\frac{\lambda_A}{\lambda_{LI}}\epsilon^* = \frac{\lambda_A}{\lambda_{LII}}\epsilon^* \qquad (22)$$

Equation (21) shows the origin of the subchannel based parameter C_1, and equation (22) is the reason why we have only one eddy parameter ϵ_1^* versus two conduction parameters ${}^{S}K_{NII}$ and ${}^{S}K_{SII}$

$$\text{i.e.} \quad \epsilon_1^* \equiv \frac{\lambda_A}{\lambda_{LI}}\epsilon^* \cong \frac{\lambda_A}{\lambda_{LII}}\epsilon^* \ ; \ \alpha^*_1 = \lambda_A\alpha^* \qquad (8\ a,\ 8\ b)$$

$$C_1 = \frac{\lambda_A}{\lambda_{LII}} C \qquad (23\ a)$$

and

$${}^{S}K_{NII} = \frac{{}^{P}K_{NII}}{\lambda_{LI}} = {}^{S}K_{NI} \qquad (8\ c)$$

$${}^{S}K_{SII} = \frac{{}^{P}K_{SII}}{\lambda_{LII}} \qquad (23\ b)$$

Proceeding to eliminate the dependance of the subchannel parameter on flow split, we divide equation (21) by S^X_{II} yielding

$$\left(\frac{S\mathbb{P}_{SII} \; P\mathbb{P}_{NII}}{S^A_{II}}\right) \frac{C_l}{S^X_{II}} \frac{\partial h^*}{\partial s^*} + \frac{\partial h^*}{\partial z^*} = D_{e_l}\left(\frac{\mathbb{P}_{NII}}{S^A_{II}}\right)\left(\frac{1}{S^X_{II}} \frac{\lambda_A}{\lambda_{LI}} \epsilon^* + \frac{P\mathbb{K}_{NII} \lambda_A \alpha^*}{S^X_{II} \lambda_{LI}}\right) \nabla^2 h$$

$$+ D_{e_l}\left(\frac{\mathbb{P}_{SII}}{S^A_{II}}\right)\left(\frac{1}{S^X_{II}} \frac{\lambda_A}{\lambda_{LII}} \epsilon^* + \frac{\mathbb{K}_{P\,SII} \lambda_A \alpha^*}{S^X_{II} \lambda_{LII}}\right) \nabla^2 h + \frac{S^{Q^*}_{II}}{S^X_{II}} \tag{24}$$

where we now define $C_{lL} \equiv \frac{C_l}{S^X_{II}}$ (25)

Additional eddy and molecular diffusivity parameters could also be defined from Eqn. (24) but for a consistent nomenclature one should return to our basic approach and redefine ϵ and α values from start with that system. Again in practice we have not yet found it necessary to retain such generality since C_{lL} has been deduced from salt conductivity data (i.e. source term zero) where the mixing parameters have been determined from the bundle inner channels. Hence the approximations have been made that

$$\epsilon^*_{lL} \equiv \frac{1}{S^X_l} \frac{\lambda_A}{\lambda_{LI}} \epsilon^* \cong \frac{1}{S^X_{II}} \frac{\lambda_A}{\lambda_{LI}} \epsilon^*$$

$$\cong \frac{1}{S^X_{II}} \frac{\lambda_A}{\lambda_{LII}} \epsilon^* \tag{26}$$

2.2.1 - Continuum representation (C_L)

Again for completeness of definitions we observe that the continuum swirl parameter independent of bundle size is obtained by dividing equation (17) by $\frac{U_{AII}}{U_A}$ which from equation (20 a) is itself equal to

$$\frac{U_{AII}}{U_A} = S^X_{II} \frac{\lambda_{AII}}{\lambda_A} \tag{27}$$

yielding

$$\left(\frac{\mathbb{P}_{SII}\, P_{NII}}{P^A_{II}}\right) \frac{1}{S^X_{II}} \frac{\lambda_A}{\lambda_{AII}} C \frac{\partial h^*}{\partial s^*} + \frac{\partial h^*}{\partial z^*} = \mathrm{De}_1 \left(\frac{P_{NII}}{P^A_{II}}\right)\left(\frac{1}{S^X_{II}} \frac{\lambda_A}{\lambda_{AII}} \epsilon^* + \right.$$

$$\left. + \frac{P^K_{NII}}{S^X_{II}} \frac{\lambda_A}{\lambda_{AII}} \alpha^*\right) \nabla h^* + \mathrm{De}_1 \left(\frac{\mathbb{P}_{SII}}{P^A_{II}}\right)\left(\frac{1}{S^X_{II}} \frac{\lambda_A}{\lambda_{AII}} \epsilon^* + \frac{K_{II}}{S^X_{II}} \frac{\lambda_A}{\lambda_{AII}} \alpha^*\right) \nabla^2 h$$

$$+ \frac{P^{Q^*}_{II}}{S^X_{II}} \frac{\lambda_A}{\lambda_{AII}} \tag{28}$$

where $$C_L \equiv \frac{1}{S^X_{II}} \frac{\lambda_A}{\lambda_{AII}} C \tag{29}$$

and we do not assign new definitions for the eddy and molecular diffusivity terms.

The results are summarized in Tables 2 and 3. Table 2 summarizes only those parameters needed for turbulent bundle analysis (i.e. the mixing factor of region I and the swirl factor of region II). Table 3 presents a complete tabulation of parameters from our foregoing development which maintains the distinctions between parameters which would become important as the mixed convection regime is entered.

2.3 POROSITY FACTORS

For a wire wrapped (one per rod) bundle in a triangular array the porosity factors of TABLE 1 are defined in terms of the following geometric factors.

D_F = duct flat to flat distance = $\left[\sqrt{3}\ PN_{RING} + D + 2\ D_W\right]$

N_{RING} = number of hexagonal rings of fuel rods in the bundle excluding the center pin which is counted as ring 0.

2.3.1 - λ_A - Bundle average axial porosity

$$\lambda_A = \frac{\text{void area}}{\text{total area}} = \frac{\frac{\sqrt{3}}{2} D_F^2 - \frac{N\pi}{4}\left(D^2 + \frac{D_w^2}{\cos\theta}\right)}{\frac{\sqrt{3}}{2} D_F^2} \tag{30}$$

assume that the fuel rod pitch P can be approximated by

$$P \cong D + D_W \tag{31}$$

then (30) becomes

$$\lambda_A = 1 - \frac{N\pi}{2\sqrt{3}} \frac{\left[\left(\frac{D}{P}\right)^2 + \frac{1}{\cos\theta}\left(1 - \frac{D}{P}\right)^2\right]}{\left[\sqrt{3}\ N_{RING} + 2 - \frac{D}{P}\right]^2} \tag{32}$$

where

$$\cos\theta = \frac{H}{\sqrt{\pi^2 (D+D_w)^2 + H^2}} \tag{32a}$$

2.3.2 λ_{AI} - Region I Axial Porosity

$$\lambda_{AI} = \frac{\frac{\sqrt{3}}{2} P \frac{1}{2} P - \frac{1}{2}\frac{\pi}{4}\left(D^2 + \frac{D_w^2}{\cos\theta}\right)}{\frac{\sqrt{3}}{2} P \frac{1}{2} P} \tag{33}$$

2.3.3 λ_{AII} - Region II Axial Porosity

$$\lambda_{AII} = \frac{\text{Region II void area}}{\text{Region II total area}} = \frac{\text{Region II total area - Region II area for rods and wires}}{\text{Bundle total area - Region I total area}}$$

$$= \frac{\frac{\sqrt{3}}{2} D_F^2 - \frac{\sqrt{3}}{2} (D_F - D - 2D_w)^2 - \pi \left(D^2 + \frac{D_w^2}{\cos\theta}\right) - \frac{3}{4}\pi \left(D^2 + \frac{D_w^2}{\cos\theta}\right)(N_{RINGS} - 1)}{\frac{\sqrt{3}}{2} D_F^2 - \frac{\sqrt{3}}{2} (D_F - D - 2D_w)^2}$$

$$= 1 - \frac{\frac{(D^2 + D_w^2)}{\cos\theta}\left(\pi + \frac{3}{4}\pi (N_{RINGS} - 1)\right)}{\frac{\sqrt{3}}{2}\left[D_F^2 - (D_F - D - 2D_w)^2\right]} \qquad (34)$$

2.3.4 λ_{LI} - Minimum lateral porosity (Region I)

$$\lambda_{LI} = \frac{\text{lateral cross flow area}}{\text{pitch length}} = \frac{P - D}{P} = 1 - \frac{D}{P} \qquad (35)$$

2.3.5 λ_{LII} - Minimum lateral porosity (Region II)

$$\lambda_{LII} = \frac{D_g}{D_g + \frac{D}{2}} \qquad (36)$$

assume that D_g is given by

$$D_g = \frac{1}{2}(1 - F) \cdot T_{ff} + D_w \qquad (37)$$

then equation (36) becomes

$$\lambda_{LII} = \frac{\frac{1}{2}(1 - F) \cdot T_{ff} + D_w}{\frac{1}{2}(1 - F) \cdot T_{ff} + D_w + \frac{D}{2}} \qquad (38)$$

2.4 CONVERSION AMONG MIXING AND SWIRL PARAMETERS

It may often be necessary to convert between the parameter definitions of Table 2 to obtain input in the form required. Table 2 illustrates that the conversion process requires evaluation of ratios of porosities which in general vary with P/D and bundle size. Two cases are shown below:

2.4.1 ε^* to ε_1^*

Equation (8a) relates these parameters as

$$\varepsilon_1^* = \frac{\lambda_A}{\lambda_{LI}} \varepsilon^* \tag{39}$$

The ratio $\frac{\lambda_A}{\lambda_{LI}}$ is obtained from equations (32) and (35) as

$$\frac{\lambda_A}{\lambda_{LI}} = \left[1 - \frac{N\pi}{2\sqrt{3}} \frac{\left[\left(\frac{D}{P}\right)^2 + \frac{1}{\cos\theta}\left(1 - \frac{D}{P}\right)^2\right]}{\left[\sqrt{3}\, N_{RING} + 2 - \frac{D}{P}\right]^2}\right] \left[\frac{1}{\left[1 - \frac{D}{P}\right]}\right] \tag{39a}$$

is presented graphically in Fig. (2) as a function of P/D and the number of fuel rods, N, for the case of H/D = 16.

Notice that $\frac{\lambda_A}{\lambda_{LI}}$ is also a function of H/D as a result of the definition of $\cos\theta$ (eqn. 32a). However, as shown in Figure 1, it is only a weak function and hence, the $\frac{\lambda_A}{\lambda_{LI}}$ ratio is not plotted as a function of H/D.

Equation (23c) relates these parameters as

$$C_1 = \frac{\lambda_A}{\lambda_{LII}} C \tag{23c}$$

The ratio $\frac{\lambda_A}{\lambda_{LII}}$ is obtained from equations (32) and (38) as

$$\frac{\lambda_A}{\lambda_{LII}} = \left[1 - \frac{N\pi}{2\sqrt{3}} \frac{\left[\left(\frac{D}{P}\right)^2 + \frac{1}{\cos\theta}\left(1 - \frac{D}{P}\right)^2\right]}{\left[\sqrt{3}\, N_{RING} + 2 - \frac{D}{P}\right]^2}\right]\left[1 + \frac{\frac{D}{2}}{\frac{1}{2}(1 - F) \cdot T_{ff} + D_w}\right] \tag{39b}$$

is presented graphically in Fig. (3) as a function of P/D and the number of fuel rods, N, for the case of $\frac{H}{D} \approx 16$. It is not plotted as a function of $\frac{H}{D}$ for the above reason.

3. FRICTION FACTORS

Subchannel friction factors are explicitly required for the mixed convection, subchannel version of ENERGY. The results of a recent model (4) which calibrated its expressions against the available literature data are presented here. Bundle friction factors in laminar and turbulent flow may be obtained from the equal pressure drop condition. The transition value may be obtained by using these component expressions in Equation (57). A computer program, WIWRAP, to calculate all of the following parameters is given in Reference 8.

3.1 Laminar Flow Correlations for f_1 and f_2

The laminar flow correlations are calibrated against the only four data sets available, so these results should be construed as preliminary.

$$f_{iL} = \frac{C_i^*}{Re_i} + \left(\frac{A_{ri}}{A'_{si}}\right)\left(\frac{De_i}{H}\right)\left(1 - \frac{D_w}{2\,De_i}\right)\frac{C_{\alpha i}}{Re_i} \tag{40}$$

where

$$A_{r_1} = \left(\pi\left(\frac{D}{2} + D_w\right)^2 - \pi D^2/4\right)/6 \tag{41}$$

$$A_{r_2} = \left(\pi\left(\frac{D}{2} + D_w\right)^2 - \pi D^2/4\right)/4 \tag{42}$$

$$A'_{s_1} = \frac{\sqrt{3}}{4}P^2 - \frac{\pi D^2}{8} \tag{43}$$

$$A_{s_1} = \frac{\sqrt{3}}{4}P^2 - \frac{\pi D^2}{8} - \frac{\pi D_w^2}{8\cos\theta} \tag{43a}$$

$$A'_{s_2} = P\left(\frac{D}{2} + D_g\right) - \frac{\pi D^2}{8} \tag{44}$$

$$A_{s_2} = P\left(\frac{D}{2} + D_g\right) - \frac{\pi D^2}{8} - \frac{\pi D_w^2}{8\cos\theta} \tag{44a}$$

' denotes bare rod quantity

$$C_1^* = \left(-336\,(P/D - 1)^2 + 340\,(P/D - 1) + 40\right)\left(\frac{A_{s_1}}{A'_{s_1}}\right)\left(\frac{De_1}{De'_1}\right)^2 \tag{45}$$

$$C_2^* = \left(-318.2\,(P/D - 1)^2 + 290.9\,(P/D - 1) + 37.4\right)\left(\frac{A_{s_2}}{A'_{s_2}}\right)\left(\frac{De_2}{De'_2}\right)^2 \tag{46}$$

$$C_{\alpha_1} = 5835(H/D)^{0.198}/(P/D)^{3.264} \quad (47)$$

$$C_{\alpha_2} = 6805(H/D)^{0.257}/(P/D)^{4.337} \quad (48)$$

$Re_i = \frac{V_A De_i}{\nu} X_{iL}$ and X_{iL} is given by equations (61) and (62) in Section 4.2.

angle θ = angle the wire makes with the vertical (see Fig. 2-4 of Ref. 6)

3.2 Turbulent Flow Correlations for f_1 and f_2

The turbulent flow correlations are calibrated against fifty-three sets of data.

$$f_{1T} = [1+C_{T1}(\frac{A_{r1}}{A'_{s1}})(\frac{De_1}{H})(\frac{(D+D_w)}{\pi^2(D+D_w)^2+H^2})]\frac{.83\ C_{f_2}}{Re_1^{.18}} \quad (49)$$

$$f_{2T} = \{1+[C_{T2}\ n \left.\frac{V_T}{V_A}\right|_{gap}]^2\}^{1.375}\ \frac{C_{f_2}}{Re_2^{.18}} \quad (50)$$

where

$$C_{T1} = 2200 \quad (51)$$

$$C_{T2} = 1.9 \quad (52)$$

$$n = PD_g/[P(D/2+D_g) - \frac{\pi D^2}{8}] \quad \text{(this function is plotted in Fig. 4)} \quad (53)$$

$$\left.\frac{V_T}{V_A}\right|_{gap} = 10.5(\frac{D_g}{P})^{0.35}\ \frac{(D+D_w)}{\sqrt{\pi^2(D+D_w)^2+H^2}}\ (\frac{A_{r2}}{A'_{s2}})^{0.5} \quad (54)$$

$$C_{f_2} = \begin{cases} .235(P/D)^{.685}(H/D)^{-.094}, & \text{all } N_p;\ .196 \text{ in.}<D<.250 \text{ in.} \quad (55a) \\ .477(P/D)^{.656}(H/D)^{-.333}, & N_p>19 \quad (55b) \\ .475(P/D)^{.645}(H/D)^{-.356}, & N_p=19 \quad .472 \text{ in.}<D<.525 \text{ in.} \quad (55c) \end{cases}$$

$Re_i = \frac{V_A De_i}{\nu} X_{iT}$, X_{iT} is given by equations (63) and (64) in Section 4.2. (56)

NOTE: $P = D+D_w$ in Eqn (49) because it is part of sin θ.

3.3 Transition Flow Correlations for f_1 and f_2

The transition flow correlations are calibrated against fifty-seven sets of data.

$$f_{i,tr} = \{ (f_{iL})^{\ell} + (f_{iT})^{\ell} \}^{1/\ell} \tag{57}$$

where f_{iL} is given by equation (40)

f_{iT} is given by either equation (49) or equation (50)

$$\ell = 1.49 \tag{58}$$

3.4 Bundle Friction Factors

$$f_{bT} = f_{2T} \, [De_b/De_2] X_{2T}^2$$

$$f_{bL} = f_{2L} \, [De_b/De_2] X_{2L}^2$$

3.5 Important User's Note

Due to inaccuracies inherent in the calibration procedure, if the preceding friction factors are used in conjunction with the flow split parameters presented below, then the equal pressure drop condition is not satisfied. It is recommended that values of the flow split parameters to be used as inputs be obtained by solving the isothermal momentum equation with the above friction factors.

4. FLOW SPLIT

The division of flow at the bundle inlet between regions or between subchannel types is required for the ENERGY continuum and subchannel versions respectively. The relationship between region and subchannel flows is presented. Finally the effect of tolerances on the results is discussed.

4.1 Region and Subchannel Flow Splits

Region notation	Subchannel notation	
$s^{X_I} = \frac{V_{AI}}{V_A} \equiv \frac{V_{A1}}{V_A}$	s^{X_1}	interior
	s^{X_2}	edge
$s^{X_{II}} \equiv \frac{V_{AII}}{V_A}$	s^{X_3}	corner

By definition region I contains only interior subchannels so that

$$s^{X_I} \equiv s^{X_1} \tag{59}$$

The relation between $s^{X_{II}}$ and s^{X_2} can be derived as follows: From a mass balance assuming constant density

$$(N_2 A_{S2} + N_3 A_{S3}) V_{AII} = N_2 A_{S2} V_{A2} + N_3 A_{S3} V_{A3}$$

$$s^{X_{II}} = s^{X_2} \frac{N_2 A_{S2}}{N_2 A_{S2} + N_3 A_{S3}} + s^{X_3} \frac{N_3 A_{S3}}{N_2 A_{S2} + N_3 A_{S3}} .$$

$$\frac{s^{X_{II}}}{s^{X_2}} = \frac{1 + \frac{s^{X_3}}{s^{X_2}} \frac{N_3 A_{S3}}{N_2 A_{S2}}}{1 + \frac{N_3 A_{S3}}{N_2 A_{S2}}} \tag{60}$$

This relation is plotted in Figure 5 which illustrates that for the plausible range of $\frac{s^{X_3}}{s^{X_2}}$ i.e. $(0.7<\frac{s^{X_3}}{s^{X_2}}<1.3)$, for bundles of 37 pins or more, $s^{X_{II}}$ can be taken equal s^{X_2}. An assumption of this sort is required because the value of s^{X_3} has not yet been determined experimentally.

4.2 Correlations for X_1 and X_2

In turbulent (6) and laminar flow (7), respectively, the flow split parameters are derived from phenomenologically based subchannel pressure drop models. A simplified method of obtaining values for the turbulent parameters is given in Reference (5).

In transition flow (7) the flow split parameters are derived from subchannel pressure drop expressions which utilize empirically determined expressions for the subchannel friction factors. All of the above results correlate experimental data for edge and interior channels. Corner data was not available so that s^{X_3} was taken as equal to s^{X_2}: the resulting uncertainty in s^{X_1} and s^{X_2} is ±1% provided that:

a) $N_p > 37$

b) $0.6 < s^{X_3}\Big|_{actual} < 1.4$

c) $1.0 < P/D < 1.4$

The recommended laminar and turbulent correlations are given in Equations (61)-(64) below and plotted in Figures (6) and (7) for special cases of interest. The transition flow split parameters are given in Equation (65) and may be obtained by reference to the friction factor expressions given in the preceding section. The computer program, WIWRAP, Ref. (8), also calculates the following parameters:

$$X_{1L} = \frac{N_1 A_{s1} + N_2 A_{s2} + N_3 A_{s3}}{N_1 A_{s1} + (N_2 A_{s2} + N_3 A_{s3}) \left[\frac{C_1' \left(\frac{A_{s1}}{A_{s1}'}\right) \left(\frac{De_1}{De_1'}\right)^2 + C_{\alpha_1} \left(\frac{A_r}{A_{s1}'}\right) \left(\frac{De_1}{H}\right) \left(1 - \frac{D_w}{2De_1}\right)}{C_2' \left(\frac{A_{s2}}{A_{s2}'}\right) \left(\frac{De_2}{De_2'}\right)^2 + C_{\alpha_2} \left(\frac{A_{r_2}}{A_{s2}'}\right) \left(\frac{De_2}{H}\right) \left(1 - \frac{D_w}{2De_2}\right)} \right] \left(\frac{De_2}{De_1}\right)^2} \quad (61)$$

$$X_{2L} = \frac{N_1 A_{s1} + N_2 A_{s2} + N_3 A_{s3}}{N_1 A_{s1} \left[\frac{C_1' \left(\frac{A_{s2}}{A_{s2}'}\right) \left(\frac{De_2}{De_2'}\right)^2 + C_{\alpha_2} \left(\frac{A_{r_2}}{A_{s2}'}\right) \left(\frac{De_2}{H}\right) \left(1 - \frac{D_w}{2De_2}\right)}{C_2' \left(\frac{A_{s1}}{A_{s1}'}\right) \left(\frac{De_1}{De_1'}\right)^2 + C_{\alpha_1} \left(\frac{A_{r_1}}{A_{s1}'}\right) \left(\frac{De_1}{H}\right) \left(1 - \frac{D_w}{2De_1}\right)} \right] \left(\frac{De_1}{De_2}\right)^2 + (N_2 A_{s2} + N_3 A_{s3})} \quad (62)$$

$$X_{1T} = \frac{A_{s_1} N_1 + A_{s_2} N_2 + A_{s_3} N_3}{A_{s_1} N_1 + \left\{ \frac{1 + C_{T1} \left(\frac{De_1}{H}\right) \left(\frac{A_{r_1}}{A_{s_1}'}\right) \left(\frac{D + D_w}{\sqrt{\pi^2 (D + D_w)^2 + H^2}}\right)^2}{1.2\{1 + [C_{T2} n \left.\frac{V_T}{V_A}\right|_{gap}]^2\}^{1.375}} \right\}^{0.571} \left(\frac{De_2}{De_1}\right)^{0.714} [A_{s_2} N_2 + A_{s_3} N_3]} \quad (63)$$

$$X_{2T} = \frac{A_{s_1} N_1 + A_{s_2} N_2 + A_{s_3} N_3}{A_{s_1} N_1 \cdot \left\{ \frac{1.2\{1 + [C_{T2} n \left.\frac{V_T}{V_A}\right|_{gap}]^2\}^{1.375}}{1 + C_{T1} \left(\frac{De_1}{H}\right) \left(\frac{A_{r_1}}{A_{s_1}'}\right) \left(\frac{D + D_w}{\sqrt{\pi^2 (D + D_w)^2 + H^2}}\right)^2} \right\}^{0.571} \left(\frac{De_1}{De_2}\right)^{0.714} + A_{s_2} N_2 + A_{s_3} N_3} \quad (64)$$

$$S^{X_{i,tr}} = \left(\frac{f_{i,tr}}{f_{b,tr}} \cdot \frac{De_i}{De_b}\right)^{.5} \quad (65)$$

Where all of the needed geometrical parameters are defined in Equations (41)-(48) and (51)-(54) which appear in sections 3.1 and 3.2, respectively.

4.3 Effect of Tolerances

The correlations proposed in this report are based on data from test bundles. All bundles except the MIT blanket bundles were represented by nominal dimensions. For the MIT blanket bundles, the actual geometry of these bundles was used to evaluate flow splits and reduce mixing data, i.e., actual average and tolerance values of pin and wire diameters and duct dimensions were used and the looseness was distributed according to a value of $F = 0.82$ (see Figure 8)

The bounding effects of tolerances have been evaluated for some cases at MIT by means of assuming all the looseness allowed by the tolerances is concentrated in the edge region ($F = 0$) and alternately that it is concentrated in the interior region ($F = 1$), see Figure 8. For the specific case of the blanket geometry, the analysis of Ref. 11 demonstrates that the hot spot temperature differences between $F = 1$ and $F = 0$ can be as much as 10-15% of the total axial temperature rise. However, the assessment of the effects of tolerances and heated rod alignment modes on bundle temperatures must be considered an unresolved area.

4.4 Important User's Note

Again due to inaccuracies inherent to the calibration procedure, the flow split parameters do not quite satisfy the continuity equation. Thus, it is recommended that the values predicted above be divided by the factor which will make them satisfy continuity.

5.0 WIRE SWEEPING CORRELATIONS

The major driving force for the sweeping flow is the local static pressure disturbance caused by the wire wraps. Consequently, the ratio of average diversion flow rate to axial flow rate can be derived as follows [6].

$$\frac{\overline{W_{ij}}H}{m_i} = C'\left(\frac{A_r}{A'_s}\right)^{1/2}\left(\frac{Gap}{\eta}\right)^{n/2}\frac{H}{\sqrt{\pi^2(D+D_w)^2+H^2}}\quad\frac{Gap(D+D_w)}{A_s}$$

The sweeping flow in the gaps between the edge and edge subchannels is different than that in the gaps between the interior and interior subchannels because of geometric characteristics. So the sweeping flow is separately correlated for two cases; one for interior-to-interior subchannel sweeping flow and the other for edge-to-edge subchannel sweeping flow. The sweeping flows between the interior and edge subchannel is derived by extending the correlation for the sweeping flow between the two interior channels.

However, C' and n cannot be determined analytically. They must be obtained from experimental data. The mixing parameters ε^*_{1L} and C_{1L} are reduced from experimental data by calibrating the energy code against the data. These parameters can in turn be converted into the parameter $\overline{W_{ij}}H/m_i$ for the two types of gaps. The conversion relationships between the parameter $\overline{W_{ij}}H/m_i$ and the mixing parameters are as follows:

$$\frac{\overline{W_{ij}}H}{m_i} = 4.41\ (1-D/P)(H/P)\frac{\varepsilon^*_1}{X_1} \qquad \text{(A-11, 55TR,Rev 2)}$$

$$\frac{\overline{W_{ij}}H}{m_i} = \frac{D_g H}{A_s}C_{1L} = \frac{D_g H}{A_s X_2}C_1 \qquad \text{(A-16, 55TR,Rev 2)}$$

The remaining question is how to get the parameters ε^*_{1L} and C_{1L} from experiments. This question can be solved by salt injection experiments based on the premises of i) the similarity between salt mixing and heat mixing in a water cooled wire wrapped assembly and ii) the similarity of heat mixing in water and in

sodium for a given wire wrapped bundle. By comparing the energy and mass conservation equations we can prove the validity of the first similarity since diffusion effects are negligible. The second one, however, differs from the first one. For a given Reynolds number and bundle geometry heat mixing in water [Ph(H_2O)] is not equal to heat mixing in sodium [Ph(Na)] where the mixing parameter P_h is defined as the sums of turbulent interchange W'_{ij} and diversion crossflow $\bar{W}_{ij}$ effects. The quantitative difference between these two parameters, which we define in terms the relative error, is

$$\text{ERRØR} \equiv \frac{P_h(H_2O) - P_h(Na)}{P_h(Na)}$$

which through algebraic manipulation (9) can be expressed as

$$\leq \frac{[W'_{ij}\ (\text{heat})]H_2O}{[W'_{ij}(\text{heat}) + \overline{W_{ij}}]Na}$$

$$\cong \frac{\dfrac{[W'_{ij}(\text{heat})]H_2O}{P_h(H_2O)}}{1 - \dfrac{[W'_{ij}(\text{heat})]H_2O}{P_h(H_2O)}}$$

This relative error is a function of P/D, H/D and Reynolds number utilizing experimental data, and a correlation for W_{ij}, the maximum expected error has been evaluated [9]. The conclusion is that the similarity between the $P_h(H_2O)$ and $P_h(Na)$ holds under the condition that $\overline{W_{ij}}$ is much larger than W'_{ij} so that the mismatch between $[W'_{ij}(\text{heat})]Na$ and $[W'_{ij}(\text{heat})]H_2O$ can be neglected for practical combinations of P/D and H/D for LMFBR test bundles, the difference between mixing parameters for water and sodium flow is very small. Hence, to quantify the coolant energy mixing process in a LMFBR bundle, salt injection experimental data has been utilized to supplement heated sodium test data. These experimental data have been correlated as presented below in the form of parameters used in the ENERGY family of codes.

5.1 Energy Code Parameters - Turbulent Flow

New correlations have replaced those used in the original issue of this report which were taken from Ref. (1). The original correlations were based purely on the experimental results, most of which pertain to large P/D ratio bundles (P/D>1.20). These correlations reflected the conclusions that ε_1^* increases as the P/D ratio increases and that C_1 is not a function of the P/D ratio. However, the new correlations for ε_{1L}^* and C_{1L} (which are numerically very close to ε_1^* and C_1) suggest that both parameters are functions of the P/D ratio and that ε_{1L}^* decreases as the P/D ratio increases. The discrepancy between the original and the new correlations of the P/D ratio effect on the parameter ε_{1L}^* (or ε_1^*) is mainly due to the fact that the low P/D ratio data (M.I.T. P/D=1.067) were not previously available. Therefore, Skok's (Cadarache's) 7-pin experimental data (P/D=1.14) was originally included in the ε_1^* correlation to make it valid for P/D$\geq$1.14. Since the sweeping flow of the interior subchannels in a 7-pin bundles does not represent the sweeping flow in a "true" interior subchannel (as discussed in Chapter 2, ref. 6), the trend originally thought to exist for the mixing parameter ε_{1L}^* may not be correct even though the original correlation predicts all the interior subchannel mixing data for bundles of 1.14$\leq$P/D<1.32 within $\pm$ 35%.

Interior-to-interior subchannels

$$\varepsilon_{1L}^* = 0.127 \left(\frac{P-D}{P'}\right)^{-0.5} \left(\frac{A_{rl}}{A'_{sl}}\right)^{0.5} \frac{(D+D_w)P^2}{\sqrt{\pi^2 (D+D_w)^2+H^2}} \left(\frac{1}{A_{sl}}\right) \qquad (66)$$

where

$$P' = P \quad \left(\text{note } \eta = \frac{\sqrt{3}}{3} P \text{ and } \left(\frac{\sqrt{3}}{3}\right)^{-0.5} \text{ is included within 0.127}\right) \qquad (67)$$

and A'_{sl}, A_{sl}, A_{rl} are defined in equations (43), (43a) and (41), respectively.

Interior-to-edge subchannels

$$\left(\frac{1}{S^X_{II}} \frac{\lambda_A}{\lambda_{LI}} \frac{\varepsilon H_{NII}}{U_A De_1}\right) = 0.127 \left(\frac{P-D}{P'}\right)^{-0.5} \left(\frac{A_{rl}}{A'_{sl}}\right)^{0.5} \frac{(D+D_w)P^2}{\sqrt{\pi^2 (D+D_w)^2+H^2}} \left(\frac{1}{A_{sl}}\right)$$

Note that the LHS parameter appears in Table 3 and has not been given a special ε type symbol.

$$\text{Where } P' = \frac{\sqrt{3}}{3.46} P + \frac{\sqrt{3}}{2} (P-D/2) \tag{69}$$

and $S^X_{II} = S^X_2$

Edge-to-edge subchannels (donor edge subchannel is not next to corner pin)

$$C_{1L} = 10.5 \left(\frac{D_g}{P'}\right)^{0.35} \left(\frac{A_{r2}}{A'_{s2}}\right)^{0.5} \frac{D+D_w}{\sqrt{\pi^2 (D+D_w)^2+H^2}} \tag{70}$$

where $P' = P$

and A'_{s2}, A_{s2}, and A_{r2} are defined in Equations (44), (44a) and (42), respectively.

Edge-to-edge subchannels (donor edge subchannel located next to a corner pin)

$$C_{1L} = 10.5 \left(\frac{D_g}{P'}\right)^{0.35} \left(\frac{A''_{r2}}{A''_{s2}}\right)^{0.5} \frac{D+D_w}{\sqrt{\pi^2 (D+D_w)^2+H^2}} \tag{72}$$

$$\text{where } A''_{s2} = P(P- \frac{D}{2}) - \frac{\pi D^2}{8} + (\frac{1}{2}(P - \frac{D}{2})^2 \tan 30° - \frac{\pi D^2}{48}) \tag{73}$$

which represents the edge plus corner subchannel areas

$$A''_{r2} = (\pi (\frac{D}{2} + D_w)^2 - \frac{\pi D^2}{4})/3 \tag{74}$$

$$P' = 2((\frac{D}{2} + \frac{D_w}{2}) \tan 30° + \frac{P}{2}) \tag{75}$$

Plots of ε^*_{1L} and C_{1L} (donor edge subchannel not next to a corner pin) are presented in Figures (9) to (12). The above ENERGY code parameters are also calculated by the computer code, WIWRAP, Ref. (8).

5.2 ENERGY Code Parameters, Laminar Flow

The turbulent sweeping flow correlations presented in the previous section have been extended to the laminar and transition flow regimes. This is accomplished by assuming that the subchannel form pressure drop is the driving force for cross flow. With the additional assumption of a parabolic subchannel velocity distribution for low Reynolds number flows, the parameters ε^*_{1L} and C_{1L} are correlated as functions of geometry and Reynolds number. The recommended correlation is based on a cross flow friction factor of the following form:

$$K_{ij} = k\, Re_b^m \tag{76}$$

where K_{ij} is the cross flow friction factor, Re_b is the bundle Reynolds number, and k and m are constants. The constant m is evaluated by assuming that the cross flow exhibits the same Reynolds number dependence as does the bundle average resultant (axial plus transverse) flow. The parameter k should be calibrated as a function of P/D; however it is currently taken as constant due to the lack of sufficient low Reynolds number mixing data available for calibration.

The following low Reynolds number mixing correlations are recommended for Reynolds numbers less than the Reynolds number at which the laminar/transition and turbulent correlations yield the same value. For higher Reynolds numbers, the turbulent correlation is recommended.

Interior-to-Interior Subchannels

$$\varepsilon^*_{1L} = 0.0091 \left(\frac{A_r}{A'_s}\right)^{0.5} Re_b^{0.35} \left(\frac{Gap}{\eta}\right)^{-0.5} \left[\sin\theta \left(\frac{D_w}{De}\right)\left(1 - \frac{D_w}{2De}\right)\right] \frac{P^2}{A_s} \tag{77}$$

where

$$Gap = P - D \tag{78}$$

$$A_r = \left[\pi (D/2 + D_w)^2 - \frac{\pi D^2}{4}\right] /6 \tag{79}$$

$$A_s = \frac{\sqrt{3}}{4} P^2 - \frac{\pi D^2}{8} - \frac{\pi D_w^{\,2}}{8 \cos\theta} \tag{80}$$

$$A'_s = \frac{\sqrt{3}}{4} P^2 - \frac{\pi D^2}{8} \tag{81}$$

$$De = 4A_s / \frac{\pi}{2} (D + \frac{D_w}{\cos \theta}) \tag{82}$$

$$\eta = P/\sqrt{3} \tag{83}$$

$$\sin \theta = \frac{\pi (D + D_w)}{\sqrt{\pi^2 (D + D_w)^2 + H^2}} \tag{84}$$

Edge-to-Edge Subchannels

$$C_{1L} = 0.81 \left(\frac{A_r}{A'_s}\right)^{0.5} Re_b^{0.35} \left(\frac{D_g}{\eta}\right)^{0.35} \left[\sin \theta \left(\frac{D_w}{De}\right) \left(1 - \frac{D_w}{2De}\right)\right] \tag{85}$$

where

$$D_g = \frac{1}{2} (1 - F) \cdot T_{ff} + D_w \tag{86}$$

$$A_r = \left[\pi \left(\frac{D}{2} + D_w\right)^2 - \frac{\pi D^2}{4}\right] /4 \tag{87}$$

$$A'_s = P \left(\frac{D}{2} + D_w\right) - \frac{\pi D^2}{8} \tag{88}$$

$$A_s = P \left(\frac{D}{2} + D_w\right) - \frac{\pi D^2}{8} - \frac{\pi D_w^2}{8 \cos \theta} \tag{89}$$

$$De = 4 A_s / [P + \frac{\pi}{2} (D + \frac{D_w}{\cos \theta})] \tag{90}$$

$$\eta = P \tag{91}$$

$$\sin \theta = \frac{\pi (D + D_w)}{\sqrt{\pi^2 (D + D_w)^2 + H^2}} \tag{92}$$

6.0 - CRITERION TO DETERMINE WHEN BUOYANCY EFFECTS ARE IMPORTANT

In reference 11 a criterion has been derived to determine when buoyancy effects are important in a wire wrapped fuel or blanket assembly operating in steady state mixed convection flow.

Buoyancy effects were determined to be important when $G_r^* \geq G_{rc}^*$. The critical value of this dimensionless group, called G_{rc}^*, has been found to be approximately 0.025 (Ref.11).

6.1 - Skewed Radial Power Profile

For an assembly operating in steady state conditions, the definition of G_r^* was determined to be as follows: (Errata to ref.11 given in COO-2245-30 are included here plus necessary change in the γ definition to terms involving ε_{1L}^* vs ε_1^* and α_{1L}^* vs α_1^*)

$$G_r^* = \frac{Gr}{f\, R_e^2}\, \chi \tag{93}$$

where

$$\chi = \frac{1}{M}\, \frac{1}{\gamma_L}\, \frac{\hat{Q}_{p-1}}{2} \tag{94}$$

$$G_r = \frac{g_o\, \beta (T_M - T_{IN})\, D_{e_1}^3}{\nu^2} \tag{95}$$

$$\gamma = \frac{(P/D-1)}{\pi}\, \frac{16}{D_F}\, (\varepsilon_{1L}^* + S K_{NI}\, \alpha_{1L}^*) \tag{96}$$

$(T_M - T_{IN})$ = average axial temperature rise across the bundle of height L

$\hat{Q}_p$ = radial power skew (peak/avg)

Re = Reynolds number in bundle based on De_1 and interior subchannel axial velocity and bundle mean axial temperature

f = friction factor determined from smooth tube conditions at Re based on definition $f \equiv \dfrac{\Delta p}{\dfrac{L}{D_{e_1}} \dfrac{\rho V_{A1}^2}{2}}$

L = bundle axial length

ν = kinematic viscousity evaluated at mean bundle temperature $(T_M + T_{IN})/2$

β = volume expansion coefficient, evaluated at mean bundle temperature

M = Novendstern's multiplication factor for wire wrapped bundle

$$= \left\{ \frac{1.034}{(P/D)^{0.124}} + \frac{29.7\ (P/D)^{6.94}\ Re^{0.086}}{(H/D)^{2.239}} \right\}^{0.885}$$

g_o = acceleration due to gravity

6.2 - Flat Radial Power Profile (From reference 12)

For the flat radial power case, $\hat{Q}_p = 1$ and $G_r^* = 0$. This leads to a conclusion that buoyancy effects are negligible. However, this is not the case for a flat radial power assembly operated at low Raynolds

number. The difference between the flow rates of the different types of subchannels can result in a temperature difference between edge and interior subchannels. The radial temperature difference thus may cause a buoyancy effect.

The basic definition of the G_r^* reported in reference 11 is

$$G_r^* = \frac{g_o \beta [T(Z) - \bar{T}(z)]}{F_D} \tag{97}$$

where

$$F_D = \frac{Mf}{De_1} \tag{98}$$

$T(Z)$ = fluid temperature in the bundle

$\bar{T}(Z)$ = mean fluid temperature

In order to predict buoyancy effects in a conservative way, the $[T(Z) - \bar{T}(Z)]$ in the above equation is replaced by $[T_{max}(L) - \bar{T}(L)]$, where $T_{max}(L)$ denotes the maximum temperature at bundle exit where the $[T(Z) - \bar{T}(Z)]$ has a maximum value. Therefore, the G_r^* becomes

$$Gr^* = \frac{g_o \beta [T_{max}(L) - \bar{T}(L)]}{F_D} \tag{99}$$

The $[T_{max}(L) - \bar{T}(L)]$ can be obtained by solving the temperature profile of a two region assembly at uniform radial power. One region contains all the interior subchannels and the other region contains all the peripheral subchannels. The governing equations for the fluid enthalpy of these two regions are:

$$m_{AI} \frac{dh_I}{dZ} = P\rho \left(\varepsilon_{H_{NI}} + {}_pK_{NI}\alpha\right) \frac{h_{II} - h_I}{\eta} + {}_p(QA)_I \qquad (100)$$

$$m_{AII} \frac{dh_{II}}{dZ} = P\rho \left(\varepsilon_{H_{NI}} + {}_pK_{NI}\alpha\right) \frac{h_I - h_{II}}{\eta} + {}_p(QA)_{II} \qquad (101)$$

Where η = centroid-to-centroid distance between region I and region II

${}_p(QA) = {}_pQ_pA$ = heat added to the region I or region II per unit length

Note ${}_p(QA)_I = {}_s(QA)_I = (QA)_I$

${}_p(QA)_{II} = {}_s(QA)_{II} = (QA)_{II}$

The solution for $h_I(L)$ and $h_{II}(L)$ in equation (100) and (101) are as follows:

$$h_I(L) = h_{IN} + \frac{\left[(QA)_I + (QA)_{II}\right] L}{m_{AI} + m_{AII}} + \left(\frac{(QA)_I m_{AII}}{(m_{AI} + m_{AII})\Theta} - \frac{\left[(QA)_I + (QA)_{II}\right]}{(m_{AI} + m_{AII})n\Theta} \right) \left(1 - e^{-n\Theta L}\right) \qquad (102)$$

$$h_{II}(L) = h_{IN} + \frac{\left[(QA)_I + (QA)_{II}\right] L}{m_{AI} + m_{AII}} + \left(\frac{(QA)_{II} m_{AI}}{(m_{AI} + m_{AII})\Theta} - \frac{\left[(QA)_I + (QA)_{II}\right]}{(m_{AI} + m_{AII})\, n\Theta} \right) \left(1 - e^{-n\Theta L}\right) \qquad (103)$$

where

$$\Theta = \frac{P\rho\ (\varepsilon_{H_{NI}} + {}_{p}K_{NI}\alpha)}{\eta} \tag{104}$$

$$n = \frac{{}^{m}_{AI} + {}^{m}_{AII}}{{}^{m}_{AI}\ {}^{m}_{AII}} \tag{105}$$

Subtracting eq.(103) from (102) we obtain

$$h_I(L) - h_{II}(L) = \frac{(QA)_I\ {}^{m}_{AII} - (QA)_{II}\ {}^{m}_{AI}}{({}^{m}_{AI} + {}^{m}_{AII})\Theta} \left(1-e^{-n\Theta L}\right) \tag{106}$$

Because $T_{max}(L) - \overline{T}(L)$ is approximately equal to the temperature of the interior region minus the average fluid temperature which can be expressed as

$$\overline{T}(L) = \frac{N_1\ {}^{m}_{AI} T_I(L) + N_2\ {}^{m}_{AII} T_{II}(L)}{N_1\ {}^{m}_{AI} + N_2\ {}^{m}_{AII}} \tag{107}$$

where N_1 = number of interior subchannels

N_2 = number of edge subchannels

$$T_{max}(L) - \overline{T}(L) = T_I(L) - \frac{N_1\ {}^{m}_{AI} T_I(L) + N_2\ {}^{m}_{AII} T_{II}(L)}{N_1\ {}^{m}_{AI} + N_2\ {}^{m}_{AII}}$$

$$= \frac{N_2\ {}^{m}_{AII}}{N_1\ {}^{m}_{AI} + N_2\ {}^{m}_{AII}} \left(T_I(L) - T_{II}(L)\right) \tag{108}$$

Inserting equation (106) into above equation, we obtain

$$T_{max}(L) - \overline{T}(L) = \left(\frac{N_2\ {}^{m}_{AII}}{N_1\ {}^{m}_{AI} + N_2\ {}^{m}_{AII}}\right)\left(\frac{(QA)_I\ {}^{m}_{AII} - (QA)_{II}\ {}^{m}_{AI}}{{}^{m}_{AI} + {}^{m}_{AII}}\right)$$

$$\left(\frac{1}{\Theta\, Cp}\right)\left(1-e^{-n\Theta L}\right) \tag{109}$$

Then equation (99) becomes

$$G_r^* = \frac{g_0 \beta \left\{ \left(\frac{N_2 {}^m A_{II}}{N_1 {}^m A_I + N_2 {}^m A_{II}} \right) \left(\frac{(QA)_I {}^m A_{II} - (QA)_{II} {}^m A_I}{{}^m A_I + {}^m A_{II}} \right) \left(\frac{1}{\theta C_p} \right) \left(1 - e^{-n\theta L} \right) \right\}}{F_D} \qquad (110)$$

In addition, since we know

$$R_e = \frac{\rho V_{A1} D_{e1}}{\mu} = \frac{V_{A1} D_{e1}}{\nu}$$

$$m_{AI} = \rho_s A_I V_{AI} = \rho_s A_1 V_{A1} = \rho_s A_1 V_A \, s^{X_1} = \rho_s A_I V_A \, s^{X_I}$$

$$m_{AI} = \rho_s A_{II} V_{AII} = \rho_s A_{II} V_A \, S^{X_{II}}$$

Equation (110) can be reformed as

$$G_r^* = \frac{g_0 \beta \left\{ \left(\frac{N_2 \, s^{A_{II}} \, s^{X_{II}}}{N_1 \, s^{A_{Is}} \, {}^{X_I} + N_2 \, s^{A_{II}} \, s^{X_{II}}} \right) \left(\frac{(QA)_{Is} {}^{X_{II}} \, s^{A_{II}} - (QA)_{IIs} {}^{X_I} s^{A_{II}}}{s^{X_{Is}} A_I + s^{X_{IIs}} A_{II}} \right) \left(\frac{1}{\theta C_p} \right) \left(1 - e^{-n\theta L} \right) \right\} D_{e_1}^3}{Mf \, Re^2 \nu^2} \qquad (111)$$

The above modified Grashof number is derived from the definition employed in Reference 11. However, whether the criteria stated in (Ref. 11) is applicable or not with respect to the above formula (i.e., a flat radial power case) has not yet been studied. In any case, if the above G_r^* number for flat radial power case is much larger than 0.025, it is reasonable to assume that the mixed convection condition will be experienced.

7.0 - IMPORTANT NOTE ON ENERGY CODE LISTING

The listing of the ENERGY codes uses "D" the rod diameter as the non-dimensionalizing parameter. However, it was later decided to use De_1 the hydraulic diameter of the interior subchannel as the characteristic dimension (as opposed to D) in order to maintain the same definition of Reynolds number as commonly used in literature. The code requires $\varepsilon^* = \frac{\varepsilon_{H_{NI}}}{U_A De_1}$ as input but converts it to $\frac{\varepsilon_{H_{NI}}}{U_A D}$ for use in the ENERGY code. The SUPERENERGY-2 document records the fact that SUPERENERGY was revised to utilize De_1 directly through the input parameter ε_1^*. The input for ENERGY code series are listed as follows for convenience.

Code	ε	C
ENERGY III	ε^*_{1L}	C_{1L}
SUPERENERGY-2	ε^*_{1L}	C_{1L}
TRANSENERGY-S (Glazer's Thesis)	ε^*_1	C_1

REFERENCES

1. E. U. Khan, W. M. Rohsenow, A. A. Sonin and N. E. Todreas. "A Porous Body Model for Predicting Temperature Distribution in in Wire-Wrapped Fuel Rod Assemblies," Nuclear Engineering and and Design 35 (1975) 1-12.

2. E. U. Khan, W. M. Rohsenow, A. A. Sonin and N. E. Todreas. "A Porous Body Model for Predicting Temperature Distribution in Wire-Wrapped Rod Assemblies Operating in Combined Forced and Free Convection," Nuclear Engineering and Design 35 (1975) 199-211.

3. B. C. Chen and N. E. Todreas. "Prediction of the Coolant Temperature Field in a Breeder Reactor Including Interassembly Heat Transfer," Nuclear Engineering and Design 35 (1975) 423-440.

4. J. T. Hawley, C. Chiu, N. E. Todreas and W. M. Rohsenow. "Subchannel and Bundle Friction Factors and Flow Split Parameters for Laminar, Transition and Turbulent Longitudinal Flows in Wire Wrap Spaced Hexagonal Arrays," COO-2245-79TR, August 1980.

5. C. Chiu, W. Rohsenow and N. Todreas. "Flow Split Model for LMFBR Wire Wrapped Assemblies," COO-2245-56 TR, REv. I, June 1980.

6. C. Chiu, W. Rohsenow and N. Todreas. "Turbulent Sweeping Flow Mixing Model for Wire-Wrapped LMFBR Assemblies," COO-2245-55 TR, Rev. 2, Dec. 1980.

7. K. J. Burns, W. M. Rohsenow, N. E. Todreas. "Laminar/Transition Sweeping Flow Mixing Model for Wire-Wrapped LMFBR Assembles," DOE/ET/37240-81TR, July 1980.

8. S. F. Wang, N. E. Todreas. "Computer Model for MIT Correlations for Friction Factors, Flow Splits, and Mixing Parameters in LMFBR Wire-Wrapped Rod Assemblies," DOE/ET/37240/87 TR, Feb. 1981.

9. C. Chiu. "Investigations in Coolant Mixing and Flow Split for LMFBR Wire Wrapped Assemblies," Ph.D. thesis, Massachusetts Institute of Technology, 1975.

10. D. S. Rowe. "COBRA-IIIC - A Digital Computer Program for Steady State and Transient Thermal Hydraulic Analysis of Rod Bundle Nuclear Reactor Elements," BNWL - 1965, March 1973.

11. E. U. Khan. "A Porous Body Model for Predicting Temperature Distributions in Wire-Wrapped Fuel and Blanket Assemblies of a Liquid Metal Fast Breeder Reactor," Sc.D. Thesis, Massachusetts Institute of Technology, January 1975. Also appears as E. U. Khan et al, "A Porous Body Model for Predicting Temperature Distributions in Wire-Wrapped Fuel and Blanket Assemblies of a Liquid Metal Fast Breeder Reactor," Departments of Mechanical and Nuclear Engineering, MIT, COO-2245-16TR, February 1975.

12. C. Chiu and N. Todreas . "WARD Blanket Assembly Pretest Predictions by SUPERENERGY," COO-2245-40TR, May 1977.

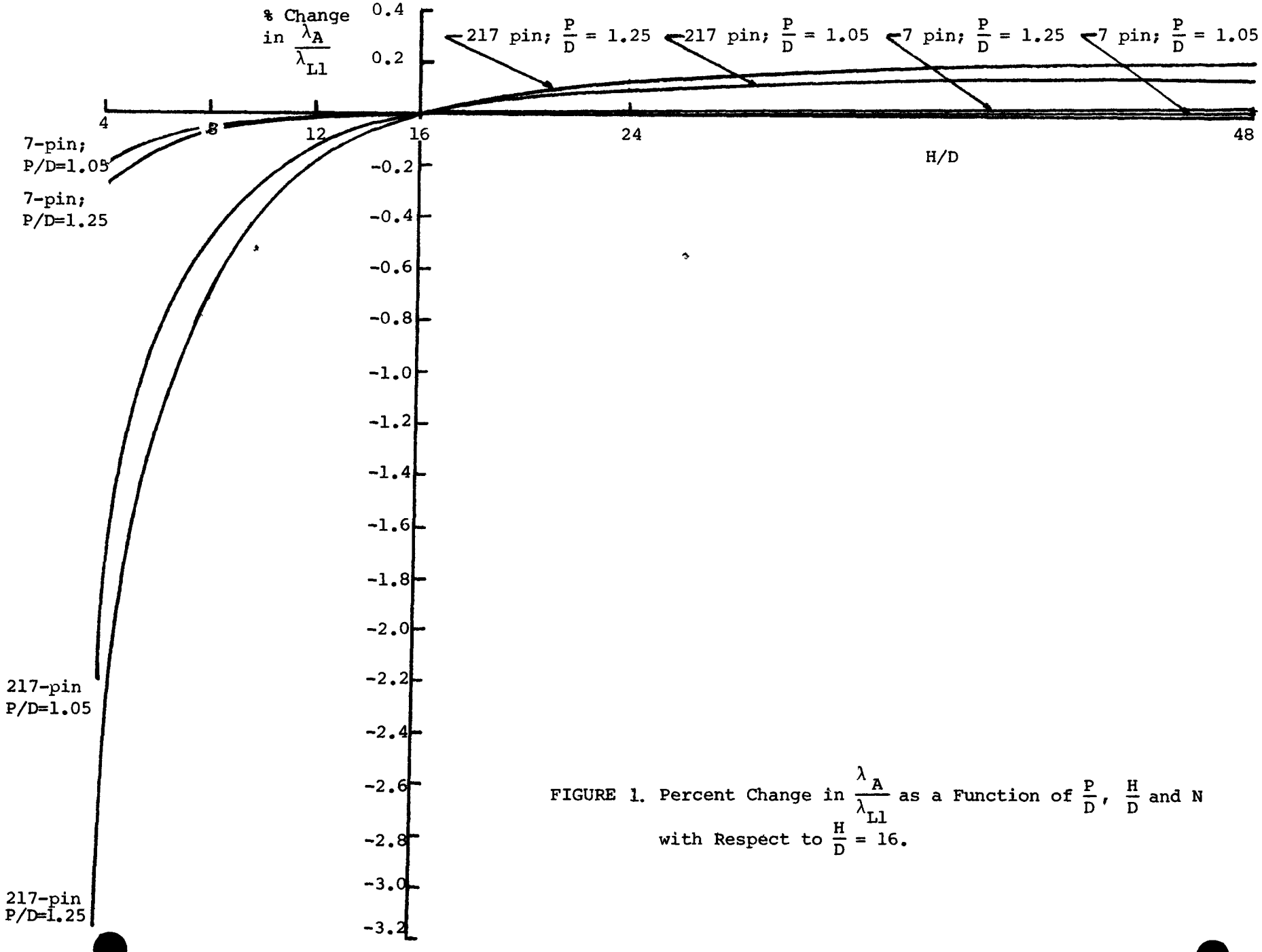

FIGURE 1. Percent Change in $\frac{\lambda_A}{\lambda_{L1}}$ as a Function of $\frac{P}{D}$, $\frac{H}{D}$ and N with Respect to $\frac{H}{D}$ = 16.

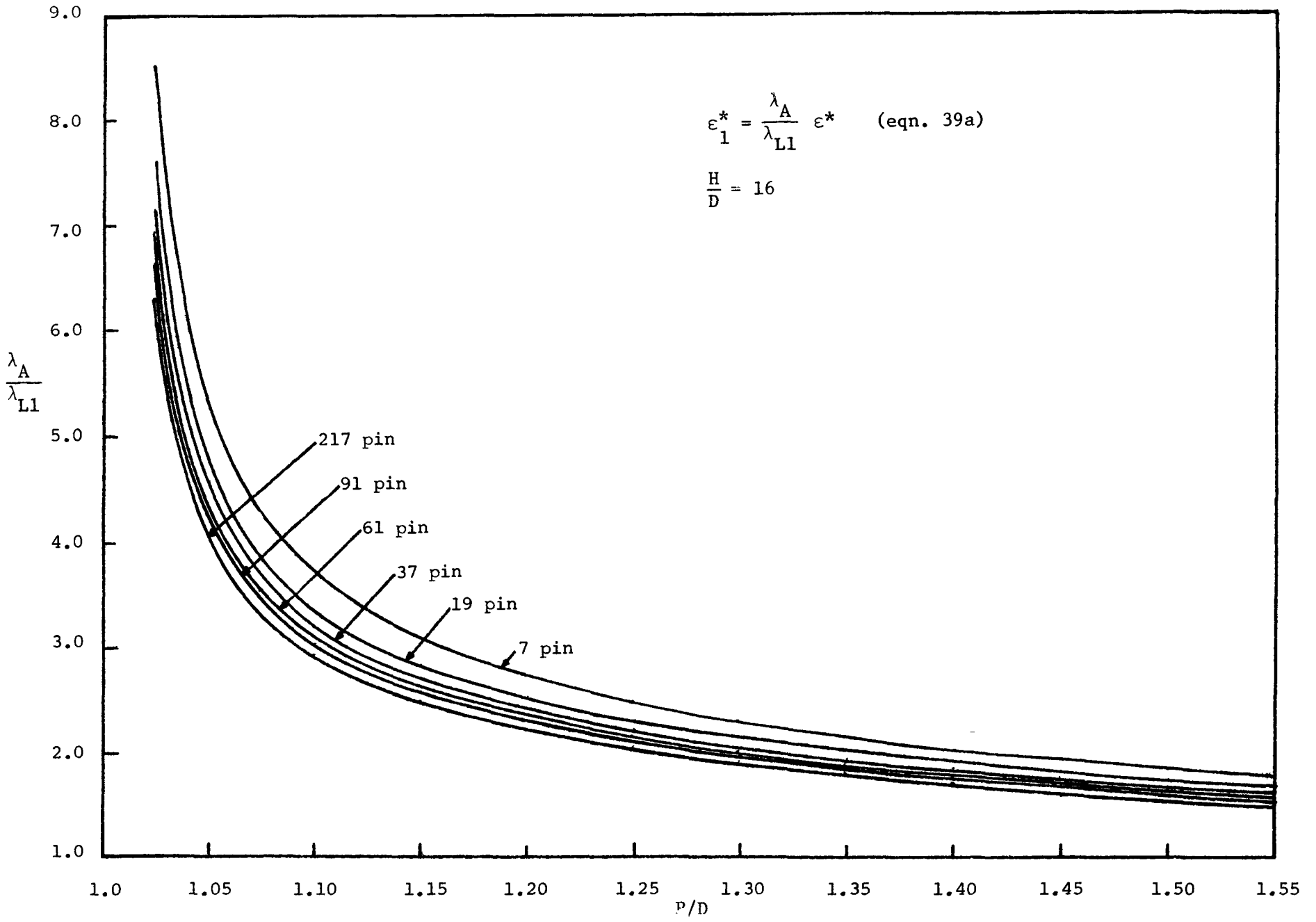

FIGURE 2. Porosity Ratio for ε_1^* to ε^* Conversion

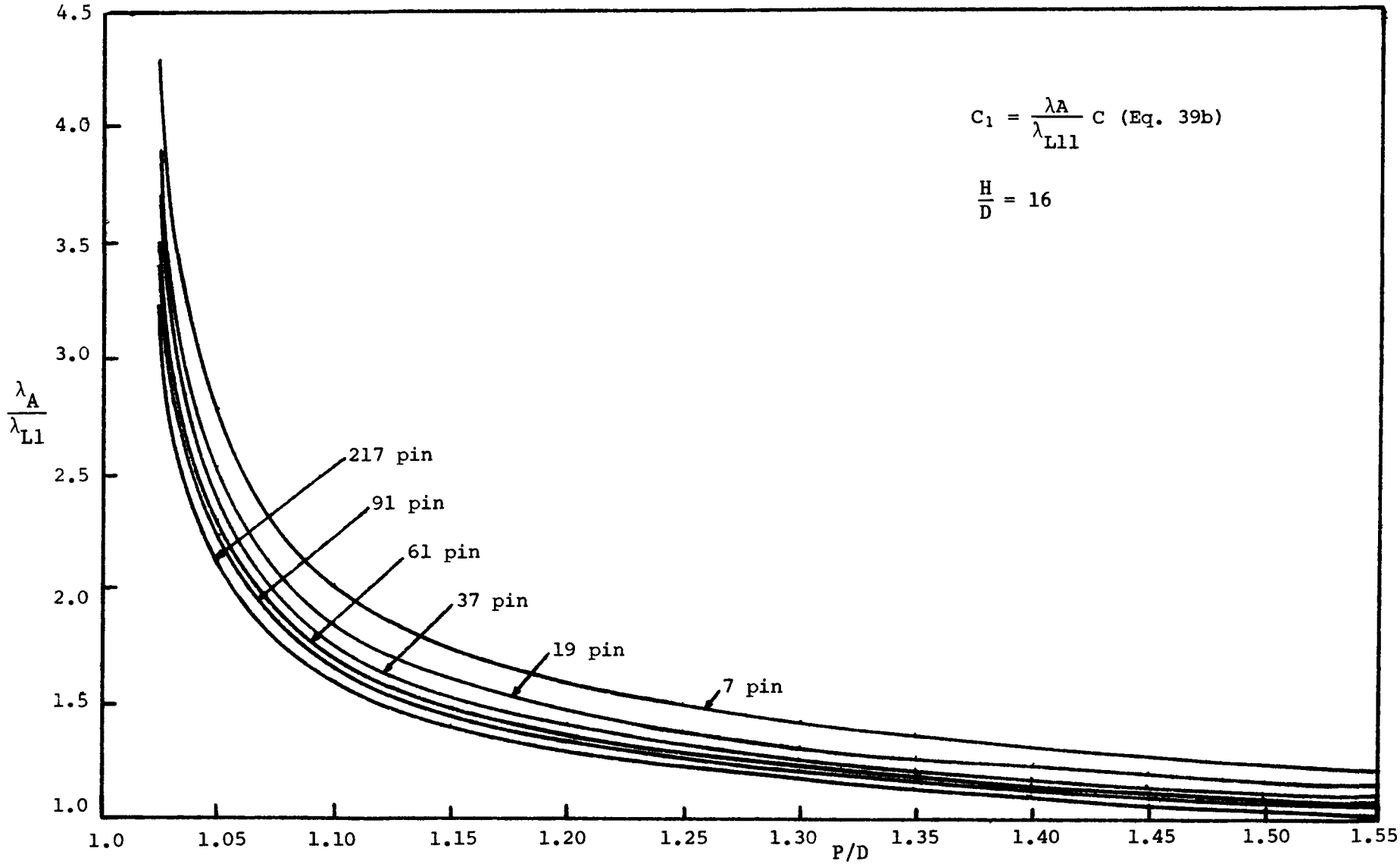

Figure 3. Porosity Ratio for C_1 to C Conversion

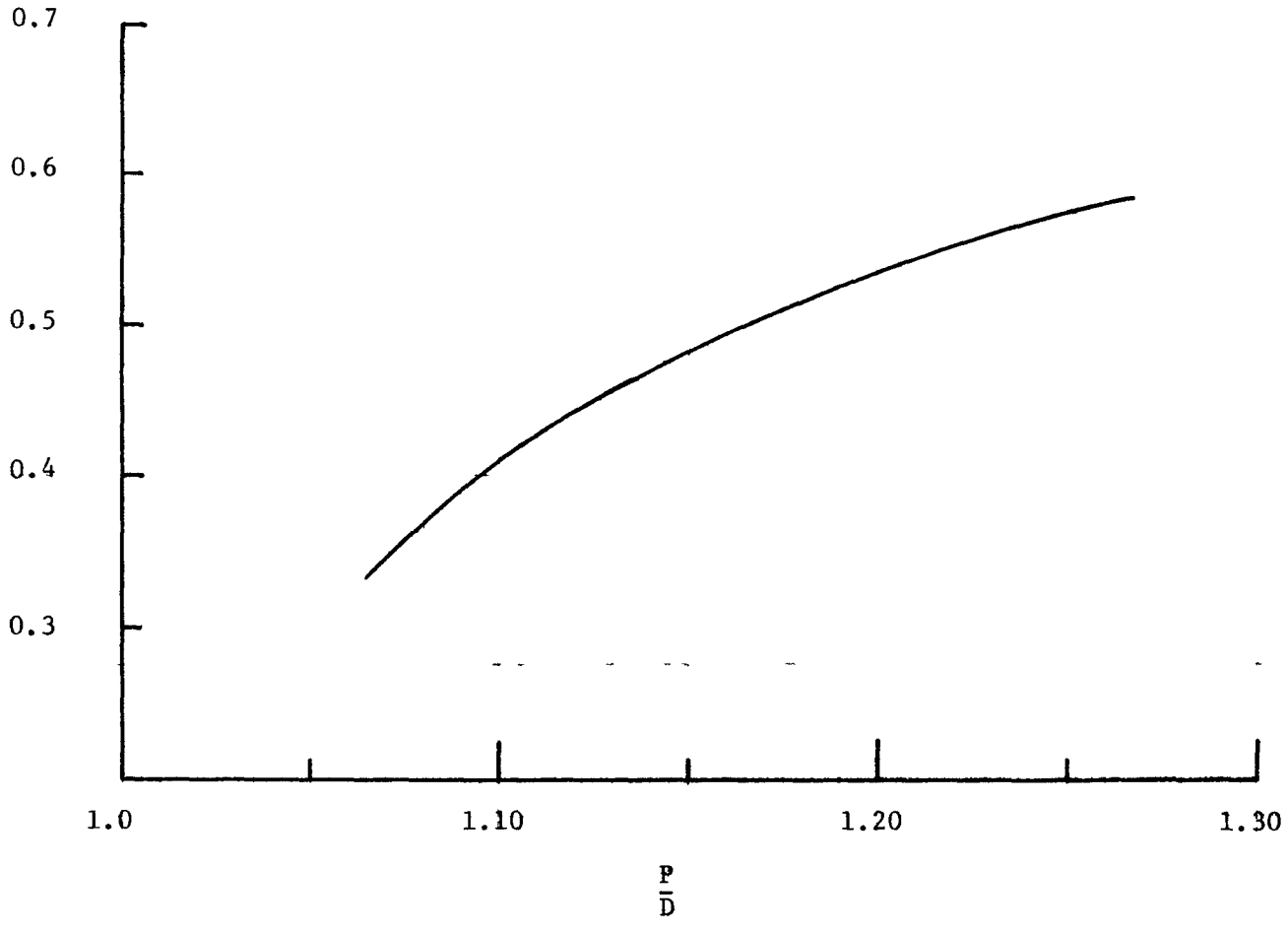

Figure 4. Parameter n in Equation (53) versus P/D Ratio

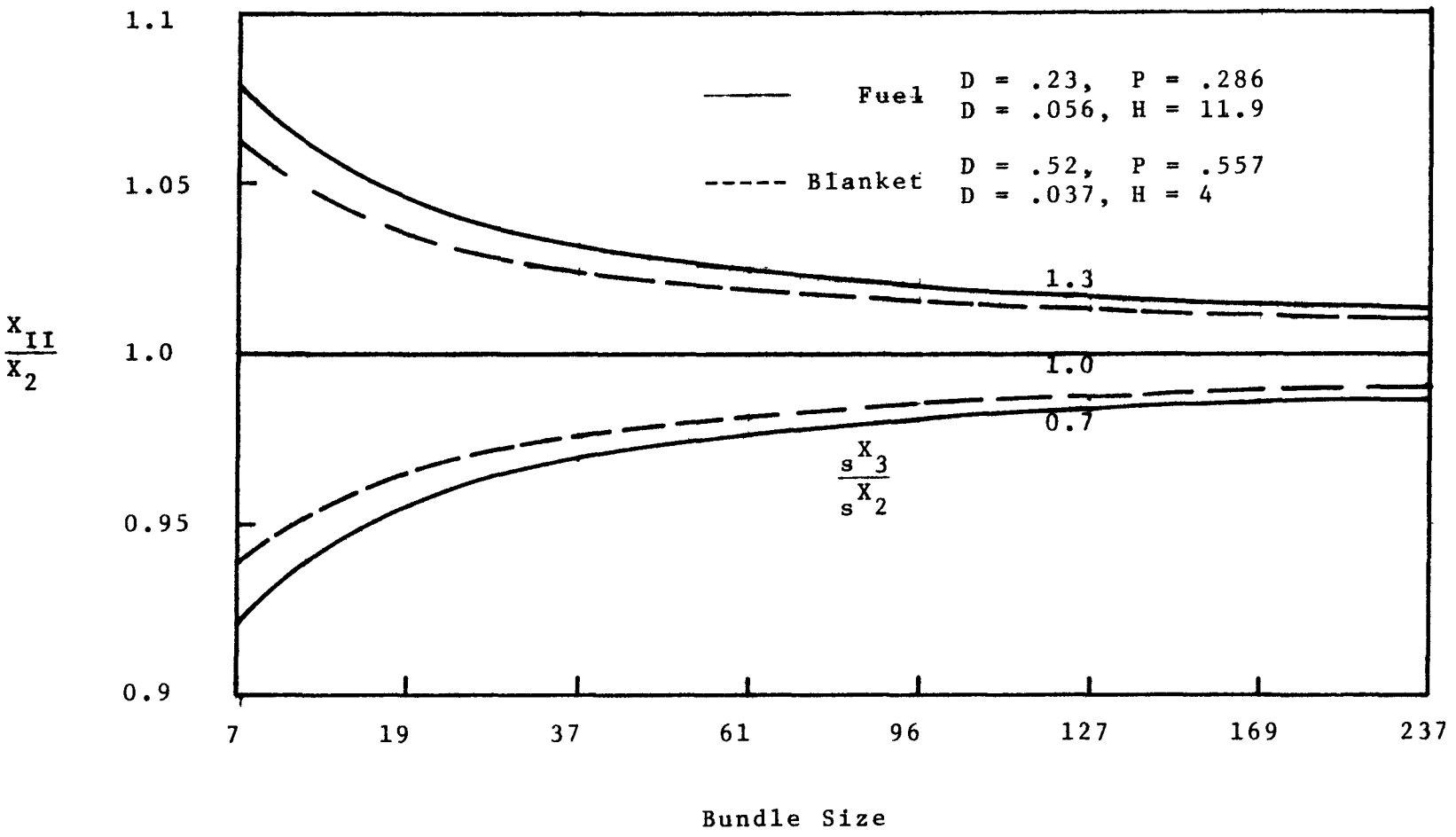

FIGURE 5. Ratio of Flow Splits for Region II and Edge Subchannels

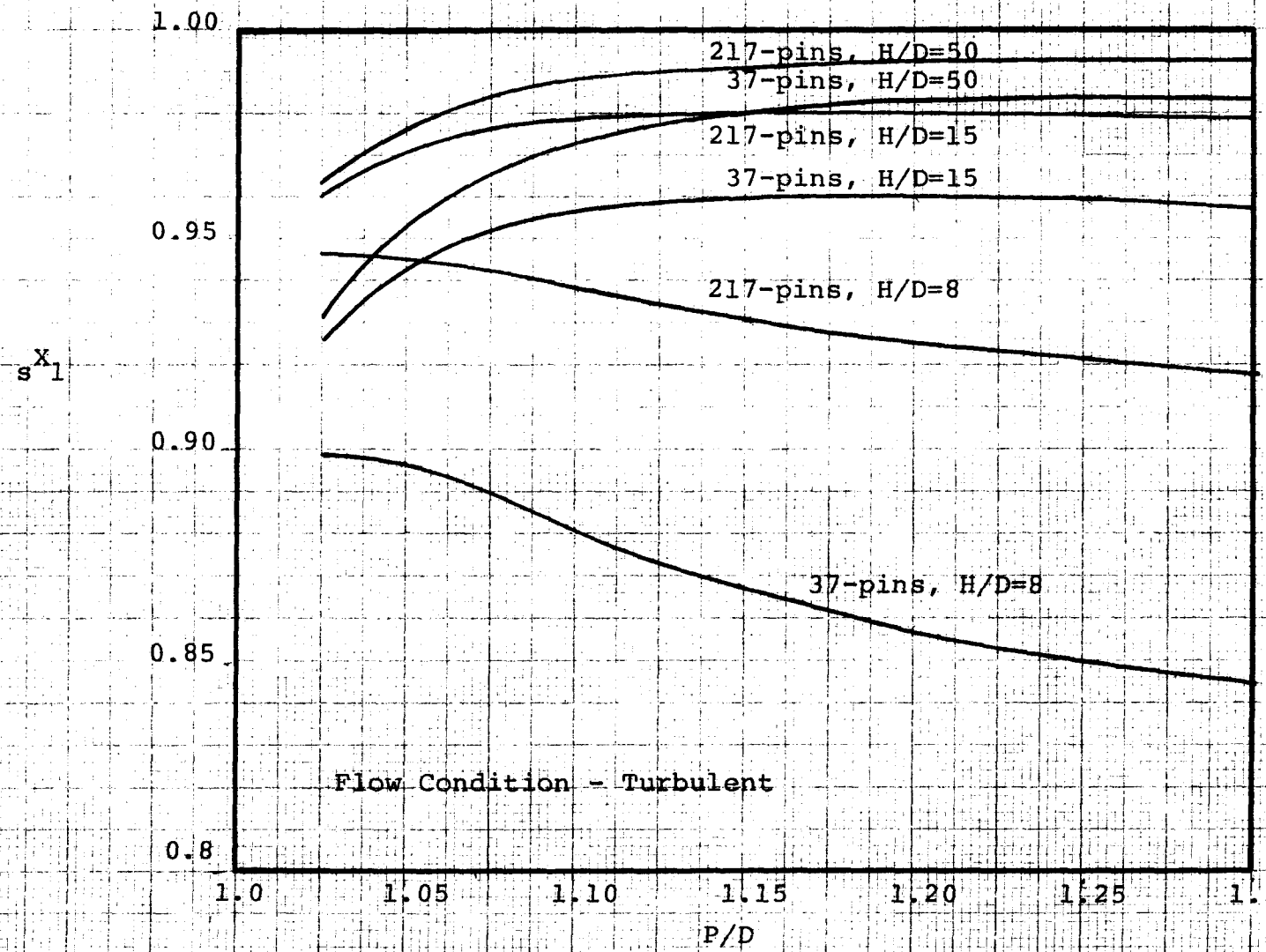

Figure 6. Predicted Interior Flow Split Parameter X_1 (Eq. 63)

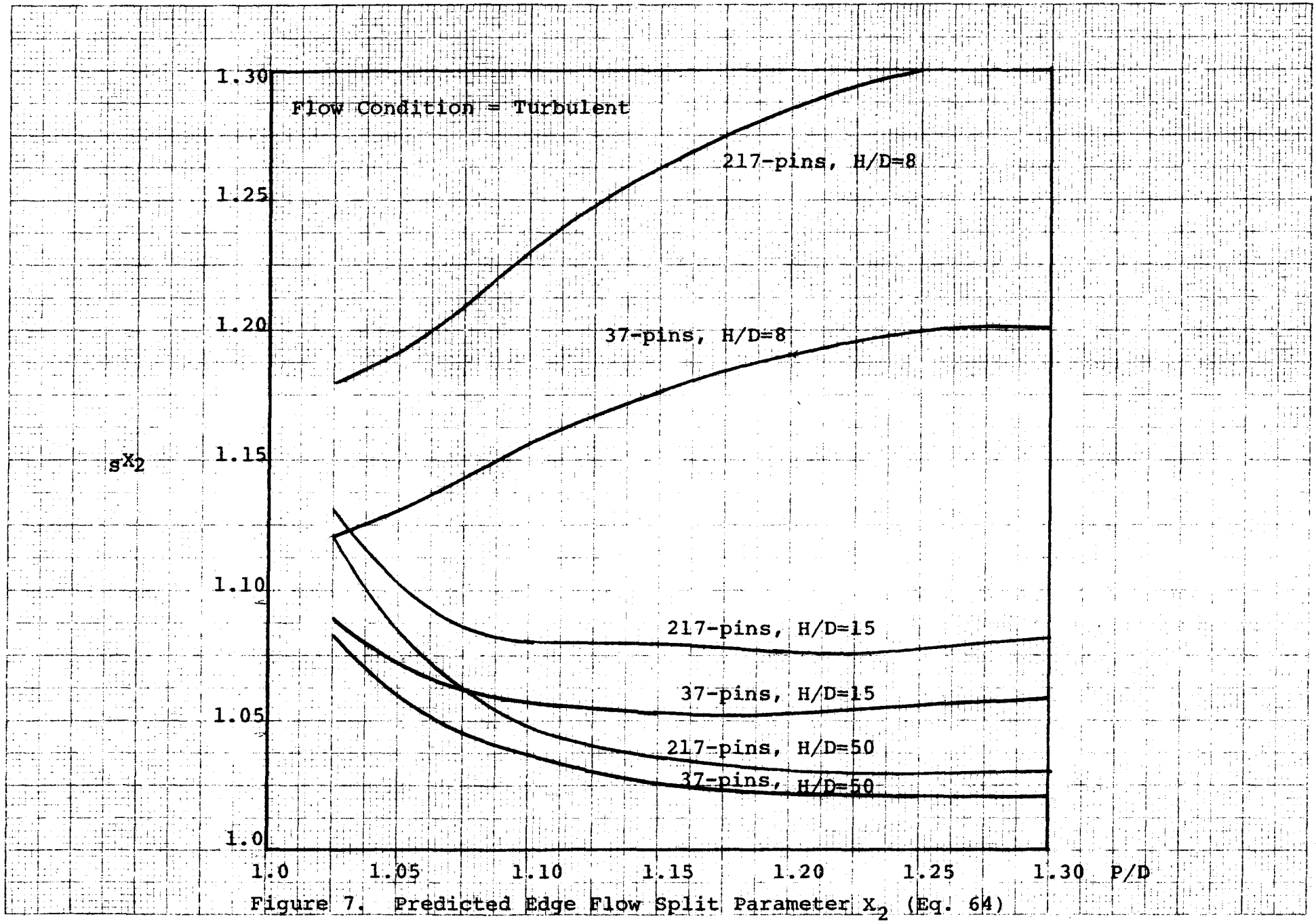

Figure 7. Predicted Edge Flow Split Parameter X_2 (Eq. 64)

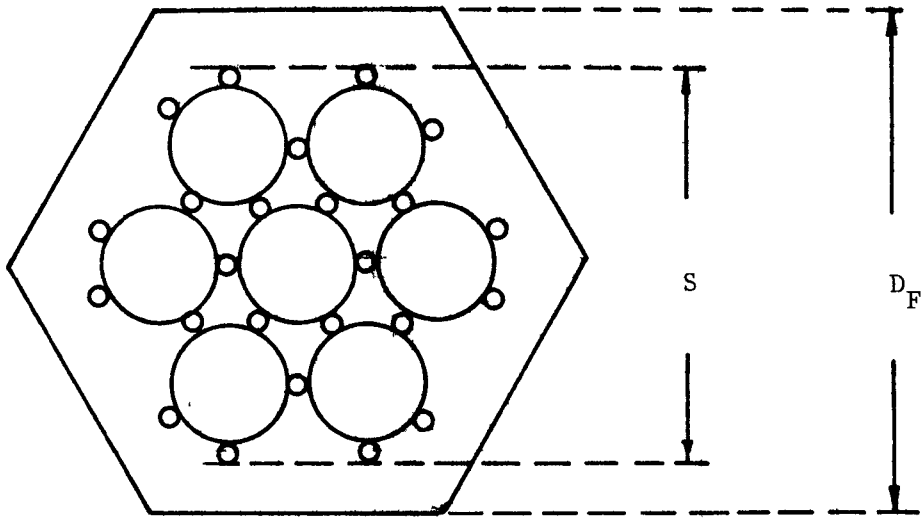

$$\text{Flat Tolerance} \equiv D_F - S$$

$$F \equiv \frac{\sqrt{3}\,(P-D-Dw)\,N_{ring}}{\text{Flat Tolerance}}$$

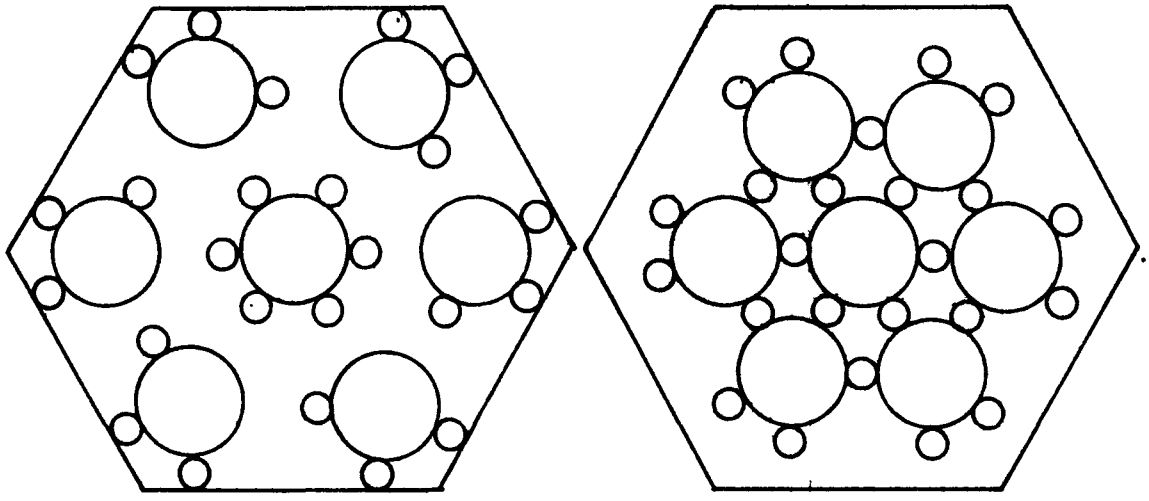

F = 1.0 F = 0

Figure 8. Definition of Flat Tolerance and Rod Alignment Modes of F = 1.0 and F = 0

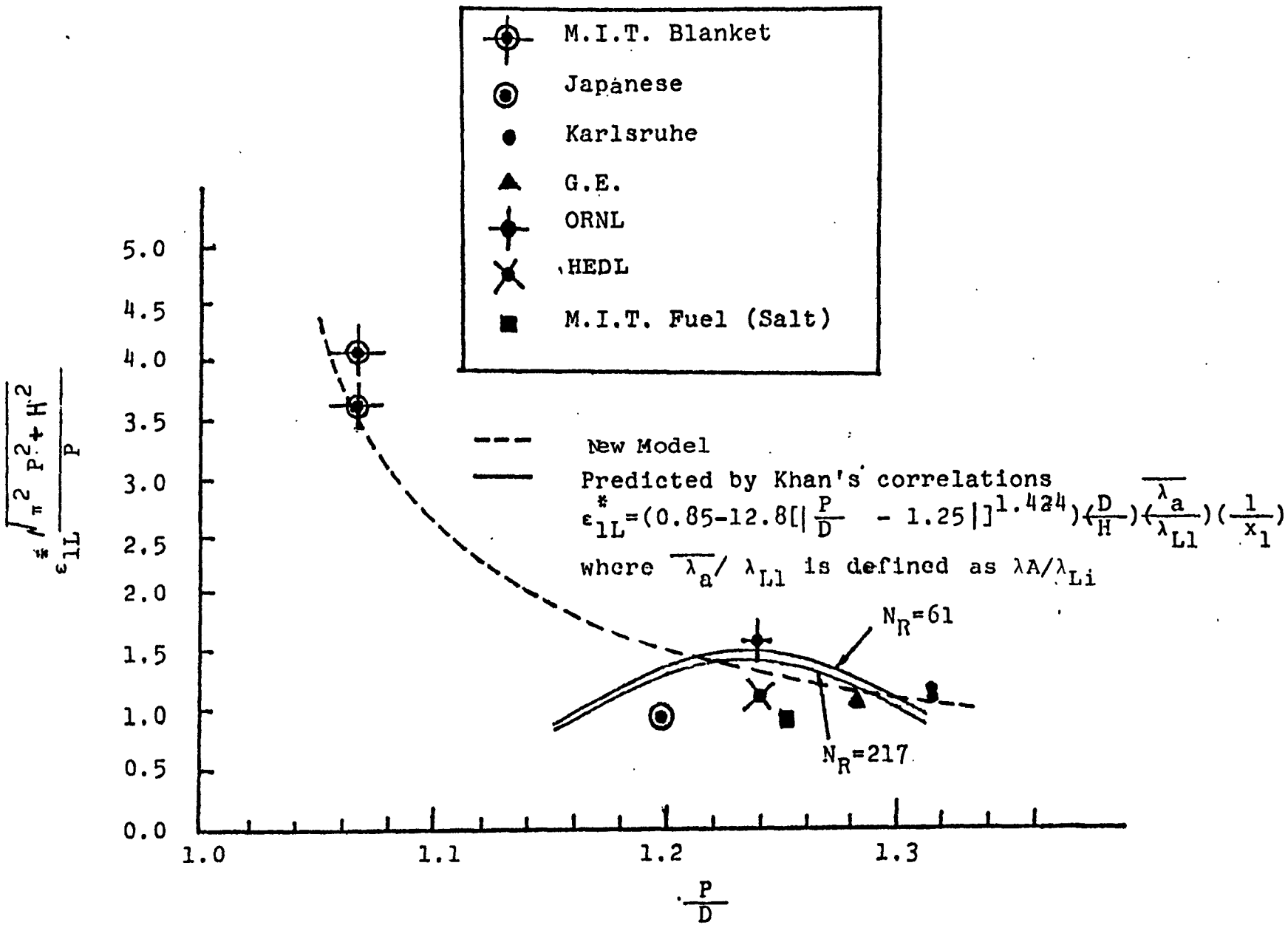

Figure 9. Comparison between Original and New Correlations for ε^*_{1L}

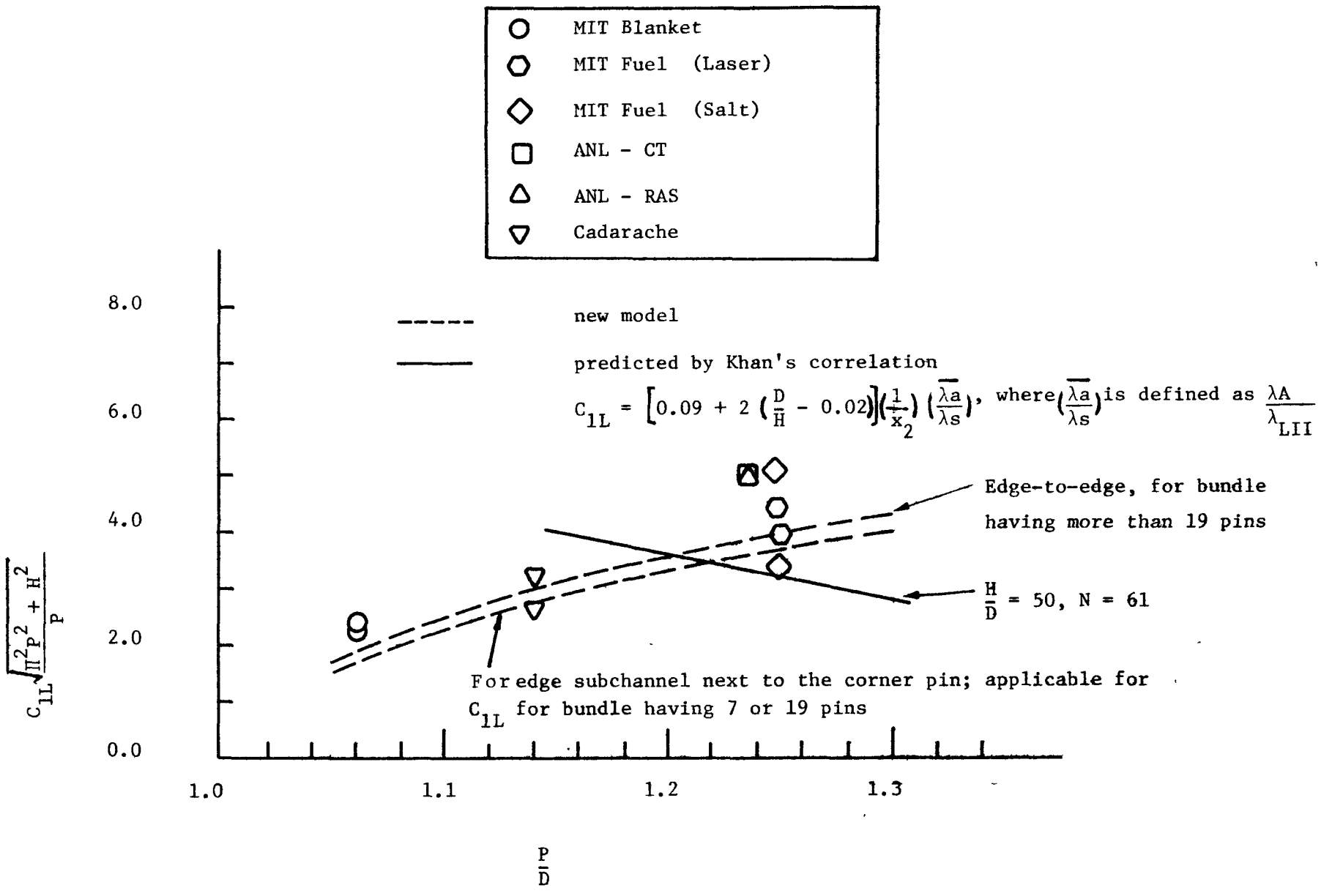

Figure 10. Comparison between Original and New Correlations for C_{1L} (N ≥ 19)

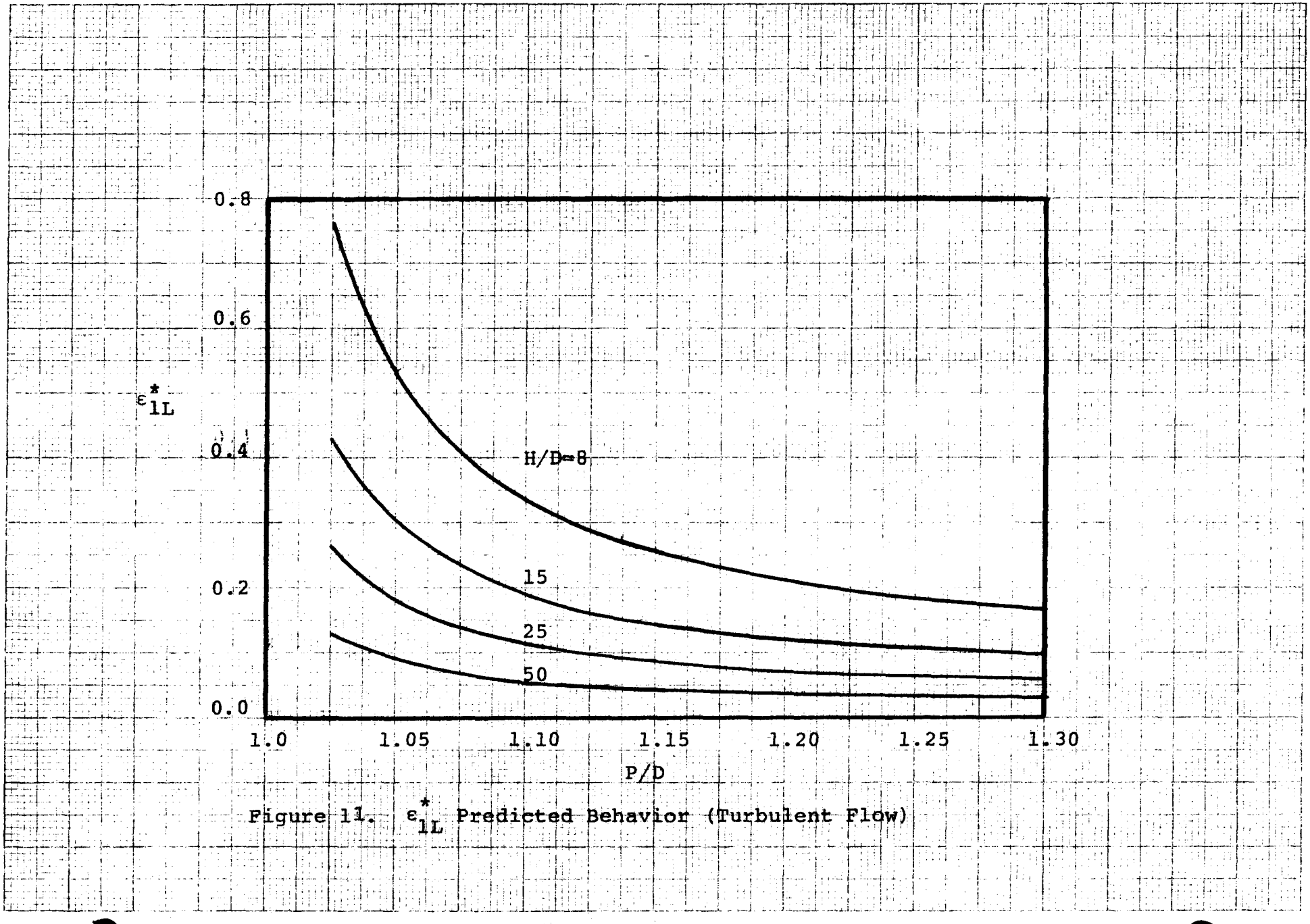

Figure 11. ε^*_{1L} Predicted Behavior (Turbulent Flow)

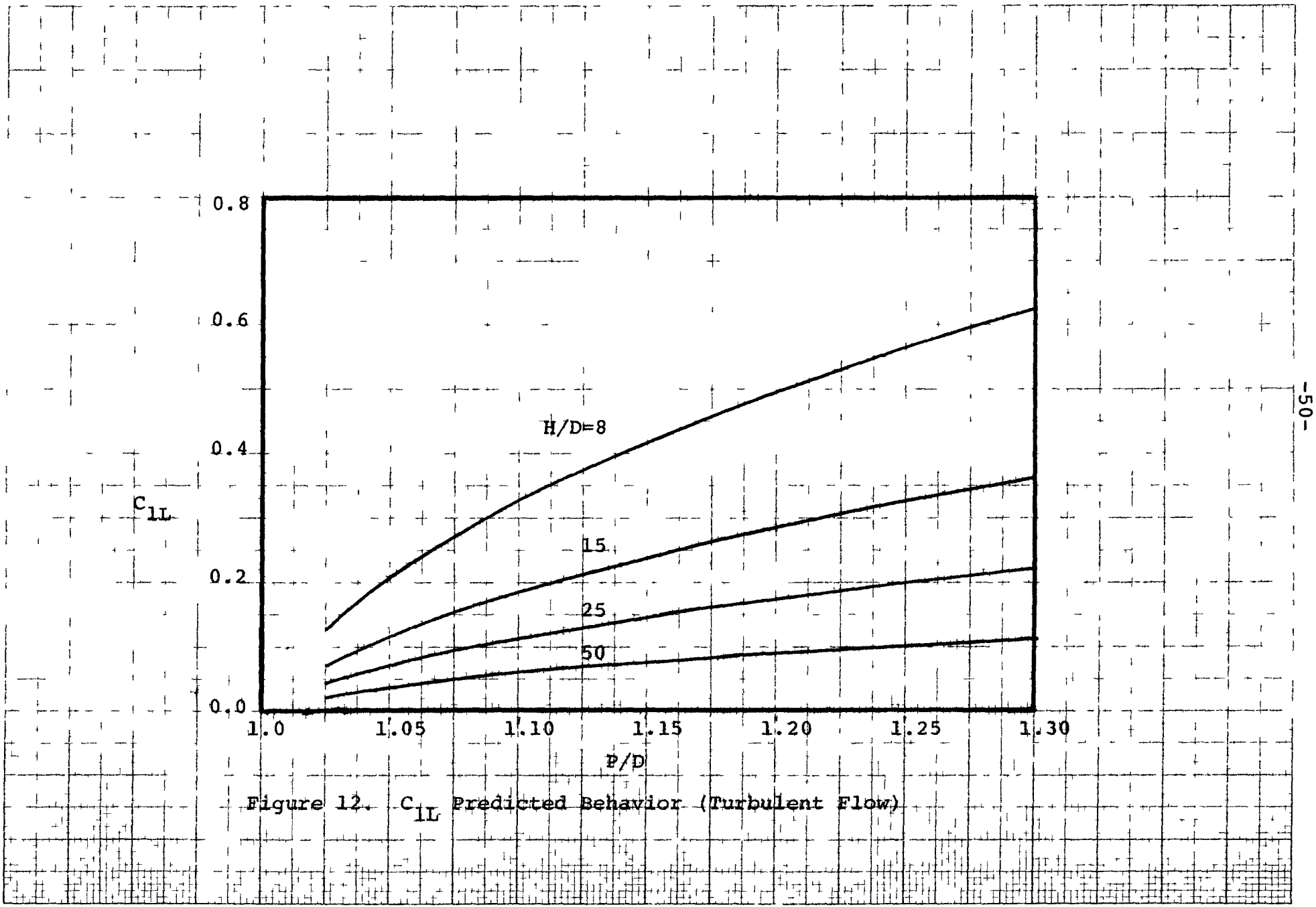

Figure 12. C_{1L} Predicted Behavior (Turbulent Flow)

TABLE 1 - POROSITY FACTORS

REGION	AXIAL POROSITY	MINIMUM LATERAL POROSITY
I	λ_{AI}	λ_{LI}
II	λ_{AII}	λ_{LII}
BUNDLE AVERAGE	λ_{A}	
ONLY THOSE POROSITIES NEEDED IN THE ANALYSIS ARE DEFINED		

TABLE 2 - PARAMETERS FOR TURBULENT BUNDLE ANALYSIS

	REPRESENTATION	
	CONTINUUM	SUBCHANNEL
BUNDLE SIZE DEPENDENT PARAMETERS	$\epsilon^* = \frac{\epsilon_{H_{NI}}}{U_A D_{e_I}}$ (4 a) $C = \frac{U_{SII}}{U_A}$ (18)	$\epsilon^*_I = \frac{\lambda_A}{\lambda_{LI}} \epsilon^*$ (8 a) $C_I = \frac{\lambda_A}{\lambda_{LII}} C$ (23 c)
BUNDLE SIZE INDEPENDENT PARAMETERS	$\epsilon^*_L = \frac{1}{S^X_I} \frac{\lambda_A}{\lambda_{AI}} \epsilon^*$ (13 a) $C_L = \frac{1}{S^X_{II}} \frac{\lambda_A}{\lambda_{AII}} C$ (29)	$\epsilon^*_{IL} = \frac{1}{S^X_I}$ [illegible] (10 a) $C_{IL} = \frac{C_I}{S^X_{II}}$ (25)

TABLE 3 - COMPLETE TABLE OF PARAMETERS FOR BUNDLE ANALYSIS

		REPRESENTATION					
		CONTINUUM			SUBCHANNEL		
BUNDLE SIZE DEPENDENT PARAMETERS	REGION I	$\epsilon^* = \frac{\epsilon_{H_{NI}}}{U_A D_{e_I}}$ (4a)	$\alpha^* = \frac{\alpha}{U_A D_{e_I}}$ (4b)	$K_{P_{NI}}$ (3)	$\epsilon^*_I = \frac{\lambda_A}{\lambda_{LI}} \epsilon^*$ (8a)	$\alpha^*_I = \lambda_A \alpha^*$ (8b)	$K_{S_{NI}} = \frac{K_{P_{NI}}}{\lambda_{LI}}$ (8c
	REGION II	$\square = \frac{\epsilon_{H_{NII}}}{U_A D_{e_I}}$ (15)	$\alpha^* = \frac{\alpha}{U_A D_{e_I}}$ (4b)	$K_{P_{NII}}$ (17)	$\square = \frac{\lambda_A \epsilon_{H_{NII}}}{\lambda_{LII} U_A D_{e_I}}$ (21 without of 16)	$\alpha^*_I = \lambda_A \alpha^*$ (8b)	$K_{S_{NII}} = \frac{K_{P_{NII}}}{\lambda_{LI}} = K_{S_{NI}}$ (8c)
		$\square = \frac{\epsilon_{H_{SII}}}{U_A D_{e_I}}$ (15)	$\alpha^* = \frac{\alpha}{U_A D_{e_I}}$ (4b)	$K_{P_{SII}}$ (17)	$\square = \frac{\lambda_A \epsilon_{H_{SII}}}{\lambda_{LII} U_A D_{e_I}}$ (21 without approx of 16)	$\alpha^*_I = \lambda_A \alpha^*$ (8b)	$K_{S_{SII}} = \frac{K_{P_{SII}}}{\lambda_{LII}}$ (23 b)
		$C = \frac{U_{SII}}{U_A}$ (18)			$C_I = \frac{\lambda_A}{\lambda_{LII}} C$ (23c)		
BUNDLE SIZE INDEPENDENT PARAMETERS	REGION I	$\epsilon^*_L = \frac{1}{S^X_I} \frac{\lambda_A}{\lambda_{AI}} \epsilon^* = \frac{\epsilon^*}{P^X_I}$ (13a)	$\alpha^*_L = \frac{1}{S^X_I} \frac{\lambda_A}{\lambda_{AI}} \alpha^*$ (13b)	$K_{P_{NI}}$ (12)	$\epsilon^*_{IL} = \frac{1}{S^X_I} \frac{\lambda_A}{\lambda_{LI}} \epsilon^* = \frac{\epsilon^*_I}{S^X_I}$ (10a)	$\alpha^*_{IL} = \lambda_A \alpha^* = \frac{\alpha^*_I}{S^X_I}$ (10 b)	$K_{S_{NI}} = \frac{K_{P_{NI}}}{\lambda_{LI}}$ (8 c)
	REGION II	$\square = \frac{1}{S^X_{II}} \frac{\lambda_A \epsilon_{H_{NII}}}{\lambda_{AII} U_A D_{e_I}}$ (28 without approx of 16)	$\square = \frac{1}{S^X_{II}} \frac{\lambda_A}{\lambda_{AII}} \alpha^*$ (28)	$K_{P_{NII}}$ (28)	$\square = \frac{1}{S^X_{II}} \frac{\lambda_A \epsilon_{H_{NII}}}{\lambda_{LI} U_A D_{e_I}}$ (24 without approx of 16)	$\square = \frac{\lambda_A}{S^X_{II}} \alpha^*$ (24)	$K_{S_{NII}} = \frac{K_{P_{NII}}}{\lambda_{LI}} = K_{S_{NII}}$ (8c
		$\square = \frac{1}{S^X_{II}} \frac{\lambda_A \epsilon_{H_{SII}}}{\lambda_{AII} U_A D_{e_I}}$ (28 without approx of 16)	$\square = \frac{1}{S^X_{II}} \frac{\lambda_A}{\lambda_{AII}} \alpha^*$ (28)	$K_{P_{NII}}$ (28)	$\square = \frac{1}{S^X_{II}} \frac{\lambda_A \epsilon_{H_{SII}}}{\lambda_{LII} U_A D_{e_I}}$ (24 without approx of 16)	$\square = \frac{\lambda_A}{S^X_{II}} \alpha^*$	$K_{S_{SII}} = \frac{K_{P_{SII}}}{\lambda_{LII}}$ (23b)
		$C_L = \frac{1}{S^X_{II}} \frac{\lambda_A}{\lambda_{AII}} C$ (29)			$C_{IL} = \frac{C_I}{S^X_{II}}$ (25)		

where $\square$ indicates that no defining symbol has been assigned.